Joint Detection and Localization in Distributed MIMO Radars Employing Waveforms With Imperfect Auto- and Cross-Correlation

Yangming Lai, *Student Member, IEEE*, Luca Venturino, *Senior Member, IEEE*, Emanuele Grossi, *Senior Member, IEEE*, and Wei Yi, *Senior Member, IEEE*

***Abstract*—This article deals with the problem of joint detection and localization of multiple targets in a distributed multiple-input multiple-output radar system where the emitted waveforms present imperfect auto- and cross-correlation functions. In this context, the sidelobe masking effects can considerably degrade the detection and localization performance of correlation-based detectors. To address this issue, we first derive a convenient discrete-time signal model, wherein the echoes generated by a target towards each receive antenna are regarded as a subspace signal. Then, we formulate the joint detection and localization problem as a composite multiple hypothesis test and derive the optimal solution according to a generalized information criterion, whose complexity scales exponentially with the number of prospective targets. To reduce the computational burden, we derive two iterative approximate solutions which detect and localize one target at a time from the noisy data, upon mitigating the sidelobe masking caused by the previously-detected ones. Finally, we provide an extensive numerical analysis to demonstrate the effectiveness of the proposed solutions, even in the challenging case where an unknown number of strong and weak targets is present in the covered area.**

***Index Terms*—Distributed MIMO radar, detection and localization, generalized information criterion, generalized likelihood ratio test, subspace detection, sidelobe masking.**

Manuscript received 16 December 2022; revised 24 May 2023; accepted 1 July 2023. Date of publication 6 July 2023; date of current version 19 December 2023. The work of Yangming Lai and Wei Yi was supported in part by the National Natural Science Foundation of China under Grants 62231008, U19B2017, and 61871103, and in part by the Fundamental Research Funds of Central Universities under Grant ZYGX2020ZB029. The work of Luca Venturino and Emanuele Grossi was supported in part by the Italian Ministry of University and Research (Dipartimenti di Eccellenza 2018-2022 Grant and PRIN 2022 Grant). An earlier version of this paper was presented at the 2022 IEEE Sensor Array and Multichannel Signal Processing Workshop (SAM), Trondheim, Norway. The review of this article was coordinated by Prof. Xianbin Wang. *(Corresponding author: Luca Venturino.)*

Yangming Lai and Wei Yi are with the School of Information and Communication Engineering, University of Electronic Science and Technology of China, Chengdu 611731, China (e-mail: ymlai1996@gmail.com; kussoyi@gmail.com).

Luca Venturino and Emanuele Grossi are with the Department of Electrical and Information Engineering (DIEI), University of Cassino and Southern Lazio, 03043 Cassino, Italy, and also with the Consorzio Nazionale Interuniversitario per le Telecomunicazioni, 43124 Parma, Italy (e-mail: l.venturino@unicas.it; e.grossi@unicas.it).

Digital Object Identifier 10.1109/TVT.2023.3293023

I. Introduction

MULTIPLE-INPUT multiple-output (MIMO) radars transmitting linearly-independent waveforms have recently attracted a large interest for both civil and military applications [1], [2], [3], [4]. In a co-located MIMO radar, the antennas are closely-spaced at both the transmit and receive sides and see the same target aspect angle [5], [6], [7], [8]; accordingly, waveform diversity and/or frequency diverse arrays can be exploited for adaptive beam-pattern shaping and signal processing. A distributed MIMO radar, instead, has widely-spaced antennas, which can see different aspect angles of the targets: the resulting spatial and geometric diversity can be exploited to reduce the scintillation of the radar cross section (RCS) [9], [10], [11], and a multidimensional measurement space can be obtained by separating all transmit-receive paths [3]. Distributed MIMO radars have been effectively used to accomplish target detection [12], [13], [14], localization [15], [16], [17], and tracking [18]; in particular, the system geometry [19], antenna placement [20], the power allocation [21], and the waveform/code design [22] can be in principle optimized to run the desired task.

There are two main approaches to perform target detection and/or localization in the distributed MIMO radars [23]. In the first approach [15], [16], [17], each receiver first obtains some position-related parameters of the detected targets, such as for example the angles and times of arrival of the corresponding echoes; then, a fusion center collects these estimated parameters and identifies the targets via triangulation. This two-step process usually requires a low transmission bandwidth and computational burden, but its performance may be degraded by the presence of missed detections and/or estimation errors at some receivers. In the second approach, the raw data measurements of all receivers are directly sent to the fusion center and jointly processed [24], [25], [26], [27], [28], [29], [30], [31]: since no preliminary elaboration is locally performed by each receiver, this solution can provide better detection and/or localization performance, especially when the signal-to-noise ratio (SNR) is low, at the price of a larger signaling overhead and computational cost. In this study, we consider this second approach, and the next paragraph analyzes the related works in more detail.

The studies in [24], [25], [26] rely on maximum likelihood (ML) estimates of the target parameters to develop localization algorithms, while [27], [28] employ grid-search methods to

obtain an estimate of the target position; however, these works assume the existence of only one target and omit the detection phase. On the other hand, surveillance radars are often faced with the problem of detecting an unknown number of prospective targets at unknown locations. The joint detection and localization (JDL) of multiple targets poses two major challenges. One challenge is that the reflections of multiple targets may interfere with each other, resulting in the creation of shadow and ghost targets; the other one is that expanding the search space to account for the presence of multiple targets much increases the computational burden. In this context, [29] has employed data and geometric matching algorithms to address the first issue. Also, [31] has employed the energy modeling of the multiple transmit-receive paths and the compressive sensing theory to address the second issue. Finally, [30] has attempted to consider both challenges simultaneously; however, the proposed correlation-based solutions rely on the assumption that the radiated waveforms have thumb-tack auto-correlation functions and all-zero cross-correlation functions, whereby the echoes produced by different waveforms or possessing different delays can be perfectly separated by a matched filter (MF). In practice, no waveform of duration T can have a thumb-tack auto-correlation function: indeed, the auto-correlation is zero only for lags exceeding T, while, for lags smaller than T, a convenient waveform design can mitigate to some extent but not eliminate the sidelobes. Also, N distinct waveforms have all-zero cross-correlation functions for all lags of interest only if they are sufficiently well separated in time or if they occupy non-overlapping frequency intervals; however, this requires an N-fold increment of the scan time or bandwidth for a given range resolution. When the transmit antennas employ waveforms that have a long duration to reduce the peak transmit power and that overlap both in time and frequency to reduce the scan time and the system bandwidth, then the resulting sidelobe masking effects can much degrade the performance of a correlation-based detector/estimator [32], [33], [34].

Recently, [35], [36] have attempted to model the cross-terms at the output of the MF and have studied their impact on the detection performance in a single-target scenario; instead, a delay compensation approach has been proposed in [37] to improve the detection capability. However, to the best of our knowledge, no previous work has still considered and solved the problem of JDL in a distributed MIMO radar when the employed waveforms present imperfect cross- and auto-correlation functions, even though somehow similar problems have been recently considered in different application areas. For example, [38] has considered a co-located MIMO radar and has proposed a sparse recovery algorithm to enhance the detection of weak targets overwhelmed by the sidelobes of strong ones, while an iterative interference cancellation algorithm has been developed in [39] to recover weak targets in a co-located MIMO-OFDM dual-function radar-communication (DFRC) system. Interference cancellation algorithms have been also developed in the context of passive radar systems [40], [41]: indeed, here the direct signal (from the illuminator of opportunity to the passive radar receiver) and the indirect signal (from the illuminator of opportunity to target to the passive radar receiver) may overlap both in time and frequency, whereby the sidelobes of the auto-correlation function may impair the target detection and localization performance when a MF detector is employed. Finally, [42], [43], [44], [45] have considered a DFRC system where a mmWave communication signal is employed as a source of opportunity and, upon resorting to a generalized information criterion (GIC) [46], have derived practical subspace-based detectors.

This article considers the multi-target JDL problem in distributed MIMO radars where the transmit antennas employ waveforms with imperfect auto- and cross-correlation functions. Starting from the preliminary results in [47], we derive two novel subspace procedures that are inherently robust to the range sidelobe masking problem. More specifically, the main contribution can be summarized as follows.

- We present a general signal model, where the superposition of the echoes produced by each target in response to the emitted radar waveforms is regarded as a subspace signal, whose structure is uniquely specified by the target position, once the radar geometry is given.
- Upon formulating the multi-target JDL problem as a composite multiple hypothesis test directly applied on the raw data, we first derive a GIC-based detector. While providing some interesting insights, this solution is however not practical, as its complexity scales exponentially in the (unknown) number of prospective targets.
- We then derive two approximate solutions to the aforementioned testing problem, which are referred to as the *matched subspace detector with iterative estimation of the interference subspace* (MSD-IS) and the *matched subspace detector with iterative estimation of the interference covariance matrix* (MSD-ICM). Following the same logic adopted in [45], these solutions extract one target at a time from the noisy data, upon mitigation the cross- and auto-terms caused by the previously-detected targets by resorting to a zero-forcing or an interference-plus-noise whitening filter, respectively.
- We provide a numerical study to show the merits of the proposed detectors, also in comparison with the previous solutions in [30] and some genie-aided benchmarks. The results confirm that our procedures effectively overcome the sidelobe masking produced by stronger targets on weaker ones, even in the presence of small localization errors, and are robust with respect to the increase in the number of interfering targets.

The closest related works are [30], [45]. While adopting a similar design approach, [45] considers a different problem, as the radar receiver is collocated with a communication transmitter in a monostatic DFRC system; our new detectors are instead able to handle a multi-static configuration where targets may even belong to dependent linear subspaces. On the other hand, while addressing the same problem tackled here, [30] makes several simplifying assumptions at the design stage that, as shown later, severely degrade the performance of the resulting detectors in the considered operating scenario.

The remainder of this work is organized as follows.[1] Section II presents the system description. Section III formulates the problem of joint target detection and localization and derives a decision rule based on the GIC. Section IV illustrates the proposed solutions. Section V contains the numerical analysis. Finally, Section VI gives the conclusions.

II. System Description

Consider a distributed MIMO radar with N transmit antennas located at $\{\boldsymbol{x}_n^{\rm tx}\}_{n=1}^N$ and P receive antennas located at $\{\boldsymbol{x}_p^{\rm rx}\}_{p=1}^P$, with[2] $\boldsymbol{x}_n^{\rm tx}, \boldsymbol{x}_p^{\rm rx} \in \mathbb{R}^2$; all antennas share a common time-reference and operate on the same spectrum. We denote by TX_n and RX_p the n-th transmit and the p-th receive antenna, respectively, for $n = 1, \ldots, N$ and $p = 1, \ldots, P$, and by $\tilde{s}_n(t)$ the baseband waveform emitted by the n-th transmit antenna. Hereafter, the positions of all radar antennas and the radiated waveforms are assumed known.

A. Radar Waveforms

At the design stage, we only assume that the waveforms $\{\tilde{s}_n(t)\}_{n=1}^N$ are time-limited to $[0, T]$ and essentially frequency limited to $[-W/2, W/2]$ [48] and that they possess the following properties:

P1 $f_{\max} T \ll 1$, where $f_{\max} \geq 0$ is the maximum magnitude of the Doppler shift in any target echo;

P2 the time-shifted replicas $\{\tilde{s}_n(t - \delta_n)\}_{n=1}^N$ are linearly independent for any $\delta_1, \ldots, \delta_N$.

The first property implies that the Doppler shift in the received echoes can be neglected; this is the typical case within each pulse repetition interval in pulse radars. The second property is required to maintain the delayed waveforms separable and implies $WT \geq N$; P2 much relaxes the requirement that the waveforms have all-zero cross-correlation functions, which would imply that $\{\tilde{s}_n(t - \delta_n)\}_{n=1}^N$ be orthogonal for any $\delta_1, \ldots, \delta_N$. Notice that no specific assumption is made here on the auto-correlation functions.

Several studies have investigated the problem of designing time- and/or frequency-coded waveforms possessing P2, which are commonly employed in radar and communication applications: see [49], [50], [51], [52], [53], [54] and references therein. For example, if time-coded waveforms are used, up to a scaling factor accounting for the transmitted energy, we have

$$\tilde{s}_n(t) = \sum_{\ell=1}^{L} b_{n,\ell} \psi\left(t - (\ell - 1)T_c\right) \tag{1}$$

where $\psi(t)$ is the chip waveform with support in $[0, T_\psi]$, T_c is the chip interval, $\boldsymbol{b}_n = (b_{n,1}, \ldots, b_{n,L})^\top$ is the code employed by the n-th antenna, and $T = (L-1)T_c + T_\psi$. The sequences $\{\boldsymbol{b}_n\}_{n=1}^N$ are usually chosen to have an impulse-like aperiodic auto-correlation function and a small aperiodic cross-correlation function. A common choice is to divide T into L equal chip intervals with constant amplitude and different phases to improve the efficiency of the power amplifiers: in this case, $T_c = T_\psi = T/L$ and $\psi(t) = \Pi(t/T_c)$, where $\Pi(t) = 1$ if $t \in [0, 1]$ and zero otherwise.

B. Continuous-Time Received Signal

In the presence of $K \geq 0$ point-like targets,[3] the baseband signal at the p-th receive antenna is [24]

$$\tilde{r}_p(t) = \sum_{k=1}^{K} \sum_{n=1}^{N} a_{p,n,k} \tilde{s}_n\left(t - \tau_{p,n}(\boldsymbol{x}_k)\right) + \tilde{w}_p(t) \tag{2}$$

for $p = 1, \ldots, P$, where the noise term $\tilde{w}_p(t)$ is a complex circularly-symmetric Gaussian process [55], independent across the receive antennas. The first term on the right-hand side is present only if $K \geq 1$; in this case, $a_{p,n,k}\tilde{s}_n(t - \tau_{p,n}(\boldsymbol{x}_k))$ is the echo produced by the k-th target in response to the probing $\tilde{s}_n(t)$ emitted by the n-th transmit antenna, for $k = 1, \ldots, K$ and $n = 1, \ldots, N$, where $\boldsymbol{x}_k \in \mathbb{R}^2$ is the position of the k-th target, while $a_{p,n,k} \in \mathbb{C}$ and $\tau_{p,n}(\boldsymbol{x}_k) \in [\tau_{\min}, \tau_{\max}]$ are the amplitude and the delay of the echo, respectively; also, $\tau_{\min}$ and $\tau_{\max}$ are the minimum and maximum delays in the inspected region, while

$$\tau_{p,n}(\boldsymbol{x}_k) = \|\boldsymbol{x}_p^{\rm rx} - \boldsymbol{x}_k\|/c + \|\boldsymbol{x}_n^{\rm tx} - \boldsymbol{x}_k\|/c \tag{3}$$

where c is the speed of light. The number of targets and, for $K \geq 1$, their positions and amplitudes are unknown.

The signal $\tilde{r}_p(t)$ is sent to a linear time-invariant filter, whose impulse response $\phi(t)$ has bandwidth W and support in $[0, T_\phi]$. The purpose of this filter is to remove the out-of-bandwidth noise. Let $s_n(t) = \tilde{s}_n(t) \star \phi(t)$ be the filtered waveform corresponding to the n-th transmit antenna, which has bandwidth W and support in $[0, T + T_\phi]$, for $n = 1, \ldots, N$; we assume that the filter $\phi(t)$ is chosen so that $\{s_n(t - \delta_n)\}_{n=1}^N$ remain linearly independent for any $\delta_1, \ldots, \delta_N$. Also, let $w_p(t) = \tilde{w}_p(t) \star \phi(t)$ be the filtered noise at the p-th receive antenna, for $p = 1, \ldots, P$. Then, $r_p(t) = \tilde{r}_p(t) \star \phi(t)$ can be expanded as

$$r_p(t) = \sum_{k=1}^{K} \sum_{n=1}^{N} a_{p,n,k} s_n\left(t - \tau_{p,n}(\boldsymbol{x}_k)\right) + w_p(t). \tag{4}$$

Hereafter we make the common assumption that two replicas of $s_n(t)$ with delay δ_1 and δ_2 are resolvable if $|\delta_1 - \delta_2| > 1/W$. Also, we provide the following definitions.

Definition 1: $K \geq 2$ targets located at $\{\boldsymbol{x}_k\}_{k=1}^K$ are *separable* if, for any target pair (k, q) with $k \neq q$, there exists at least one

[1] Column vectors and matrices are denoted by lowercase and uppercase boldface letters, respectively. $(\cdot)^*$, $(\cdot)^\top$, and $(\cdot)^H$ denotes conjugate, transpose, and conjugate-transpose, respectively. $\boldsymbol{I}_M$ is the $M \times M$ identity matrix. $\|\boldsymbol{a}\|$ is the Euclidean norm of the vector $\boldsymbol{a}$, while $\text{cat}\{\boldsymbol{a}_1, \ldots, \boldsymbol{a}_N\}$ is the MN-dimensional vector obtained by concatenating the M-dimensional vectors $\{\boldsymbol{a}_n\}_{n=1}^N$. $\text{diag}\{a_1, \ldots, a_N\}$ is the $N \times N$ diagonal matrix with the elements $\{a_n\}_{n=1}^N$ on the main diagonal. $\text{rank}\{\boldsymbol{A}\}$ and $\boldsymbol{A}^+$ are the rank and the pseudoinverse of the matrix $\boldsymbol{A}$. $\det\{\boldsymbol{A}\}$ is the determinant of the square matrix $\boldsymbol{A}$. Finally, i and $\star$ are the imaginary unit and the convolution operator, respectively, while $\text{E}\{\cdot\}$ denotes the statistical expectation.

[2] For simplicity, we consider a two-dimensional model.

[3] We assume at the design stage that the size of a prospective target is smaller than the range resolution. Notice that two or more close targets may even correspond in our model to different point-like scattering centers of the same extended object; in this case, clustering algorithms may be employed in the subsequent processing stages (not included in our study) to identify the presence of an extended object from the available detections.

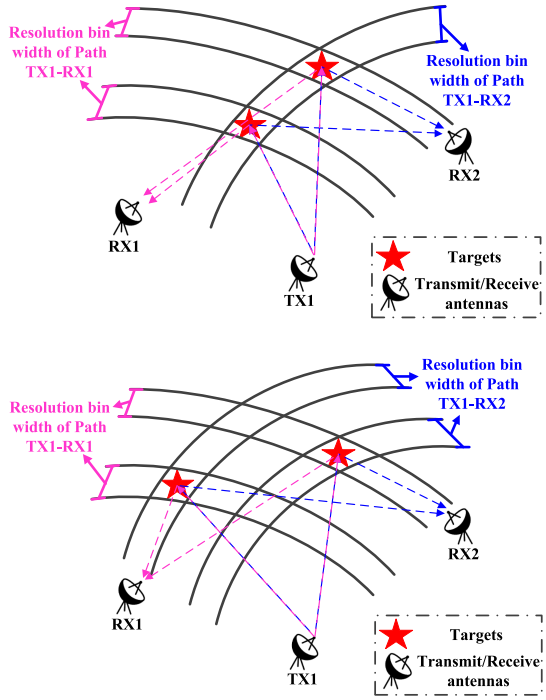

Fig. 1. Examples of separable target configurations when $K = 2$, $N = 1$, and $P = 2$. In the top plot, the targets are *partially-separable*, while in the bottom plot they are *fully-separable*.

receive/transmit antenna pair (p, n) such that $s_n(t - \tau_{p,n}(\boldsymbol{x}_k))$ and $s_n(t - \tau_{p,n}(\boldsymbol{x}_q))$ are resolvable, i.e.,

$$\min_{\substack{(k,q)\in\{1,\ldots,K\}^2 \\ k\neq q}} \max_{\substack{p\in\{1,\ldots,P\} \\ n\in\{1,\ldots,N\}}} \left|\tau_{p,n}(\boldsymbol{x}_k) - \tau_{p,n}(\boldsymbol{x}_q)\right| > \frac{1}{W}. \quad (5)$$

Definition 2: $K \geq 2$ separable targets located at $\{\boldsymbol{x}_k\}_{k=1}^K$ are said *fully-separable* if $s_n(t - \tau_{p,n}(\boldsymbol{x}_k))$ and $s_n(t - \tau_{p,n}(\boldsymbol{x}_q))$ are resolvable for any $k \neq q$ and (p, n), i.e.,

$$\min_{\substack{(k,q)\in\{1,\ldots,K\}^2 \\ k\neq q}} \min_{\substack{p\in\{1,\ldots,P\} \\ n\in\{1,\ldots,N\}}} \left|\tau_{p,n}(\boldsymbol{x}_k) - \tau_{p,n}(\boldsymbol{x}_q)\right| > \frac{1}{W}. \quad (6)$$

Otherwise, they are said *partially-separable*.

Fig. 1 reports two examples of separable target configurations. In the top plot, the two targets are *partially-separable*, as their echoes along the path originated from TX_1 and ending in RX_1 are resolvable, while those along the path originated from TX_1 and ending in RX_2 are not resolvable; in the bottom plot, instead, the two targets are *fully-separable* as their echoes are resolvable for each receive/transmit antenna pair.

C. Discrete-Time Received Signal

In the following, we process the signal received in the interval $\mathcal{I} = [\tau_{\min}, T + T_\phi + \tau_{\max})$; as shown in Fig. 2, we assume that $T + T_\phi + \tau_{\max} \leq T_{\text{pri}}$, where T_{pri} is the pulse repetition interval. $r_p(t)$ is sampled in $\mathcal{I}$ at rate $1/T_s \geq W$, thus obtaining $M = \lceil (T + T_\phi + \tau_{\max} - \tau_{\min})/T_s \rceil$ samples; notice that, under the considered assumptions, we have $M > N$. After

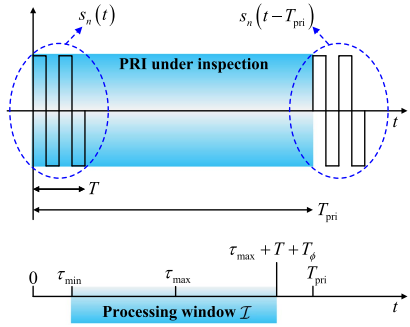

Fig. 2. Processing window.

collecting these observations into $\boldsymbol{r}_p \in \mathbb{C}^M$, we have

$$\boldsymbol{r}_p = \sum_{k=1}^{K}\sum_{n=1}^{N} a_{p,n,k}\boldsymbol{s}_{p,n}(\boldsymbol{x}_k) + \boldsymbol{w}_p$$
$$= \sum_{k=1}^{K} \boldsymbol{S}_p(\boldsymbol{x}_k)\boldsymbol{a}_{p,k} + \boldsymbol{w}_p \quad (7)$$

for $p = 1, \ldots, P$. In (7), $\boldsymbol{s}_{p,n}(\boldsymbol{x}_k)$ contains the samples $\{s_n((m-1)T_s + \tau_{\min} - \tau_{p,n}(\boldsymbol{x}_k))\}_{m=1}^M$ and represents the signature of the echo generated by the k-th target towards the p-th receive antenna when it is illuminated by the n-th transmit antenna. Also, the full-rank mode matrix $\boldsymbol{S}_p(\boldsymbol{x}_k) = [\boldsymbol{s}_{p,1}(\boldsymbol{x}_k) \cdots \boldsymbol{s}_{p,N}(\boldsymbol{x}_k)] \in \mathbb{C}^{M\times N}$ contains the signatures of the N echos of the k-th target at the p-th receive antenna,[4] while $\boldsymbol{a}_{p,k} = \text{cat}\{a_{p,1,k}, \ldots, a_{p,N,k}\} \in \mathbb{C}^N$ is the corresponding gain vector. Finally, $\boldsymbol{w}_p$ is a complex circularly-symmetric Gaussian vector with covariance $\boldsymbol{C}_p$.

For any point $\boldsymbol{x}_k$, the mode matrix $\boldsymbol{S}_p(\boldsymbol{x}_k)$ can be readily obtained, as it only depends upon the waveforms $\{s_n(t)\}_{n=1}^M$ and the positions of all transmit antennas $\{\boldsymbol{x}_n^{\text{tx}}\}_{n=1}^N$ and of the p-th receive antenna $\boldsymbol{x}_p^{\text{rx}}$, which are known. Notice also that the covariance matrices $\boldsymbol{C}_1, \ldots, \boldsymbol{C}_P$ are full-rank, as the disturbance always includes the white thermal noise of the front-end of the receiver. These matrices are assumed known in the subsequent developments; in practice an estimate could be obtained by resorting to secondary data and/or by exploiting prior knowledge of the environment.

III. Joint Target Detection and Localization

In this section, we formulate the multi-target JDL problem in a distributed MIMO radar employing waveforms with imperfect auto- and cross-correlation functions; then, we derive and discuss a GIC-based solution.

A. Problem Formulation

We aim to jointly detect and localize an unknown number of targets in the region under inspection, given only the knowledge of the radar geometry, the transmitted waveforms, and the available measurements. From (7), it is verified by inspection that $\boldsymbol{r}_p$

[4]The columns of $\boldsymbol{S}_p(\boldsymbol{x}_k)$ are linearly independent since $M > N$ and the corresponding waveforms are linearly independent by construction.

is the noisy superposition of an unknown number of *subspace signals* originated from as many targets; in particular, the k-th subspace signal belongs to the column span of $\boldsymbol{S}_p(\boldsymbol{x}_k)$, which only depends upon the position $\boldsymbol{x}_k$ of the corresponding target. We are faced here with a composite testing problem, namely,

$$\begin{cases} \mathcal{H}_0: \ \boldsymbol{r}_p = \boldsymbol{w}_p, \ \forall\, p \\ \mathcal{H}_1: \ \boldsymbol{r}_p = \boldsymbol{S}_p(\boldsymbol{x}_1)\boldsymbol{a}_{p,1} + \boldsymbol{w}_p, \ \forall\, p \\ \qquad\vdots \\ \mathcal{H}_{K_{\max}}: \ \boldsymbol{r}_p = \sum\limits_{k=1}^{K_{\max}} \boldsymbol{S}_p(\boldsymbol{x}_k)\boldsymbol{a}_{p,k} + \boldsymbol{w}_p, \ \forall\, p. \end{cases} \tag{8}$$

where $\mathcal{H}_0$ is the null hypothesis, $\mathcal{H}_K$ is the hypothesis that K targets with unknown gain vectors $\{\boldsymbol{a}_{p,1},\ldots,\boldsymbol{a}_{p,K}\}_{p=1}^{P}$ are present at the unknown positions $\boldsymbol{x}_1,\ldots,\boldsymbol{x}_K$, for $K=1,\ldots,K_{\max}$, and $K_{\max}\geq 1$ is an upper bound to the number of prospective targets.[5] As usual, we start by assuming at the design stage that the targets are located on a finite uniform grid $\mathcal{G}$ with inter-element spacing $\Delta_g \leq c/W$. Furthermore, we only search for targets which are *separable*.

The negative log-likelihood function at the p-th receive antenna is readily obtained as shown next. Under $\mathcal{H}_0$, we have

$$-\ln f_{p,0}(\boldsymbol{r}_p) = \ln\left(\pi^M \det \boldsymbol{C}_p\right) + \left\|\boldsymbol{C}_p^{-1/2}\boldsymbol{r}_p\right\|^2. \tag{9}$$

Under $\mathcal{H}_K$, for $K=1,\ldots,K_{\max}$, we have

$$\begin{aligned} &-\ln f_{p,K}\left(\boldsymbol{r}_p;\boldsymbol{x}_{1:K},\boldsymbol{\alpha}_{p,1:K}\right) = \ln\left(\pi^M \det \boldsymbol{C}_p\right) \\ &+\left\|\boldsymbol{C}_p^{-1/2}\left(\boldsymbol{r}_p - \boldsymbol{\Sigma}_p(\boldsymbol{x}_{1:K})\boldsymbol{\alpha}_{p,1:K}\right)\right\|^2 \end{aligned} \tag{10}$$

where

$$\boldsymbol{x}_{1:K} = \text{cat}\{\boldsymbol{x}_1,\ldots,\boldsymbol{x}_K\} \in \mathcal{G}_{1:K} \tag{11}$$

is the augmented vector specifying the positions of the targets,

$$\begin{aligned} \mathcal{G}_{1:K} = \{&\text{cat}\{\boldsymbol{g}_1,\ldots,\boldsymbol{g}_K\} \in \mathcal{G}^K: \\ &\min_{\substack{(k,q)\in\{1,\ldots,K\}^2 \\ k\neq q}} \max_{\substack{p\in\{1,\ldots,P\} \\ n\in\{1,\ldots,N\}}} \left|\tau_{p,n}(\boldsymbol{g}_k) - \tau_{p,n}(\boldsymbol{g}_q)\right| > 1/W\} \end{aligned} \tag{12}$$

is the set specifying all possible positions of the targets,

$$\boldsymbol{\Sigma}_p(\boldsymbol{x}_{1:K}) = \begin{bmatrix} \boldsymbol{S}_p(\boldsymbol{x}_1) & \cdots & \boldsymbol{S}_p(\boldsymbol{x}_K) \end{bmatrix} \in \mathbb{C}^{M\times KN} \tag{13}$$

is the augmented mode matrix containing the signatures of the targets, and, finally,

$$\boldsymbol{\alpha}_{p,1:K} = \text{cat}\{\boldsymbol{a}_{p,1},\ldots,\boldsymbol{a}_{p,K}\} \in \mathbb{C}^{KN} \tag{14}$$

is the augmented gain vector.

[5] $K_{\max}$ is a design parameter which depends upon the considered application. Based on its value, the other system parameters need to be properly chosen. To be more specific, notice that the received vector in (7) belongs to an M-dimensional space, while the echoes of the k-th target lays into an N-dimensional subspace. When $K=K_{\max}$, a necessary condition for correctly localizing all targets is that $K_{\max}\leq(M-N+1)$.

B. GIC-Based Solution

We solve here the JDL problem via a GIC-based approach. The likelihood function under each hypothesis is penalized to account for the model order, and an estimate of the number of targets, say $\hat{K}$, is computed as [46], [56]

$$\hat{K} = \underset{K\in\{0,\ldots,K_{\max}\}}{\arg\max}\ \text{GIC}(K) \tag{15}$$

where

$$\begin{aligned} &\text{GIC}(K) \\ &= \begin{cases} \sum\limits_{p=1}^{P} \ln f_{p,0}\left(\boldsymbol{r}_p\right), & K=0 \\ \max\limits_{\boldsymbol{x}_{1:K}\in\mathcal{G}_{1:K}} \sum\limits_{p=1}^{P} \left(\ln \dfrac{f_{p,K}\left(\boldsymbol{r}_p;\boldsymbol{x}_{1:K},\hat{\boldsymbol{\alpha}}_{p,1:K}(\boldsymbol{x}_{1:K})\right)}{f_{p,0}(\boldsymbol{r}_p)} \right. \\ \qquad \left. - \eta\,\text{rank}\left\{\boldsymbol{C}_p^{-1/2}\boldsymbol{\Sigma}_p(\boldsymbol{x}_{1:K})\right\}\right), & K\geq 1. \end{cases} \end{aligned} \tag{16}$$

In the previous equation, $\text{rank}\{\boldsymbol{C}_p^{-1/2}\boldsymbol{\Sigma}_p(\boldsymbol{x}_{1:K})\}$ specifies the model order under $\mathcal{H}_K$, while $\hat{\boldsymbol{\alpha}}_{p,1:K}(\boldsymbol{x}_{1:K})$ is the ML estimate of the augmented gain vector at the p-th receive antenna when the prospective targets are located in $\boldsymbol{x}_{1:K}$; also, η is a penalty factor which, for example, can be set to have a given probability of false alarm $\text{P}_{\text{fa}} = \Pr(\text{reject } \mathcal{H}_0 \text{ under } \mathcal{H}_0)$. Notice that $\hat{\boldsymbol{\alpha}}_{p,1:K}(\boldsymbol{x}_{1:K})$ is available in closed-form, i.e.,

$$\begin{aligned} \hat{\boldsymbol{\alpha}}_{p,1:K}(\boldsymbol{x}_{1:K}) &= \underset{\boldsymbol{\alpha}_{p,1:K}\in\boldsymbol{C}^{KN}}{\arg\min} \left\|\boldsymbol{C}_p^{-1/2}\left(\boldsymbol{r}_p - \boldsymbol{\Sigma}_p(\boldsymbol{x}_{1:K})\boldsymbol{\alpha}_{p,1:K}\right)\right\|^2 \\ &= \left(\boldsymbol{C}_p^{-1/2}\boldsymbol{\Sigma}_p(\boldsymbol{x}_{1:K})\right)^{+}\boldsymbol{C}_p^{-1/2}\boldsymbol{r}_p. \end{aligned} \tag{17}$$

Hence, upon plugging (17) into (15) and neglecting irrelevant constant terms, the GIC-based decision rule can be recast as

$$\hat{K} = \underset{K\in\{0,\ldots,K_{\max}\}}{\arg\max}\ E(K) \tag{18}$$

where $E(0)=0$,

$$\begin{aligned} E(K) = \max_{\boldsymbol{x}_{1:K}\in\mathcal{G}_{1:K}} \sum_{p=1}^{P} \left(\left\|\boldsymbol{\Pi}_p(\boldsymbol{x}_{1:K})\boldsymbol{C}_p^{-1/2}\boldsymbol{r}_p\right\|^2 \right. \\ \left. - \eta\,\text{rank}\left\{\boldsymbol{\Pi}_p(\boldsymbol{x}_{1:K})\right\}\right) \end{aligned} \tag{19}$$

for $K\geq 1$, and

$$\boldsymbol{\Pi}_p(\boldsymbol{x}_{1:K}) = \boldsymbol{C}_p^{-1/2}\boldsymbol{\Sigma}_p(\boldsymbol{x}_{1:K})\left(\boldsymbol{C}_p^{-1/2}\boldsymbol{\Sigma}_p(\boldsymbol{x}_{1:K})\right)^{+} \tag{20}$$

is the orthogonal projector onto the column span of $\boldsymbol{C}_p^{-1/2}\boldsymbol{\Sigma}_p(\boldsymbol{x}_{1:K})$. The following remarks are now in order.

Remark 1: $\boldsymbol{C}_p^{-1/2}\boldsymbol{r}_p$ is the data measured by the p-th receive antenna after a noise whitening transformation, $\|\boldsymbol{\Pi}_p(\boldsymbol{x}_{1:K})\boldsymbol{C}_p^{-1/2}\boldsymbol{r}_p\|^2$ is the energy of $\boldsymbol{C}_p^{-1/2}\boldsymbol{r}_p$ contained into the column span of $\boldsymbol{C}_p^{-1/2}\boldsymbol{\Sigma}_p(\boldsymbol{x}_{1:K})$, while $\eta\,\text{rank}\{\boldsymbol{\Pi}_p(\boldsymbol{x}_{1:K})\}$ is a penalty term that accounts for the dimension of this subspace. Accordingly, the scoring metric in (19) integrates the penalized

energies computed by each receive antenna in the candidate target subspace indexed by $\boldsymbol{x}_{1:K}$ and compares the maximum over $\mathcal{G}_{1:K}$ with a threshold; the argument of the maximum, say $\hat{\boldsymbol{x}}_{1:K} = \text{cat}\{\hat{\boldsymbol{x}}_1, \ldots, \hat{\boldsymbol{x}}_K\}$, provides an estimate of the target positions under $\mathcal{H}_K$. Finally, the rule in (18) compares the scoring metrics under all hypotheses and makes a decision on the number of targets.

Remark 2: When two or more inspected locations present a delay offset less than $1/W$ between the same transmitter and the p-th receiver, then the corresponding echoes may not be resolvable, and, consequently, $\boldsymbol{C}_p^{-1/2}\boldsymbol{\Sigma}_p(\boldsymbol{x}_{1:K})$ may be ill-conditioned. In this case, we can compute the orthogonal projector $\boldsymbol{\Pi}_p(\boldsymbol{x}_{1:K})$ in (20) from a truncated singular value decomposition of $\boldsymbol{C}_p^{-1/2}\boldsymbol{\Sigma}_p(\boldsymbol{x}_{1:K})$, wherein only the significant eigenvalues are retained, so as to avoid an unnecessary increment of the penalty term in (19).

Remark 3: For a large value of $K_{\max}$, the implementation of the GIC-based decision rule is not affordable in practice, mainly because the computation of $E(K)$ in (19) involves a search over the set $\mathcal{G}_{1:K}$ whose cardinality scales exponentially with K. More specifically, assume that the whitened mode matrix $\boldsymbol{C}_p^{-1/2}\boldsymbol{S}_p(\boldsymbol{g})$ and the whitened measurement $\boldsymbol{C}_p^{-1/2}\boldsymbol{r}_p$ are precomputed and stored into a dedicated memory, for any grid point $\boldsymbol{g} \in \mathcal{G}$ and $p = 1, \ldots, P$. Then, the computation of the orthogonal projector $\boldsymbol{\Pi}_p(\boldsymbol{x}_{1:K})$ requires a pseudoinverse, which costs at most $\mathcal{O}(MK^2\,N^2)$ floating point operations (flops), and a matrix multiplication, which costs $\mathcal{O}(M^2KN)$ flops; also, the computation of $\|\boldsymbol{\Pi}_p(\boldsymbol{x}_{1:K})\boldsymbol{C}_p^{-1/2}\boldsymbol{r}_p\|^2$ costs $\mathcal{O}(M^2)$ flops. Hence, the total cost for computing (19) is at most $\mathcal{O}((M^2KN + MK^2\,N^2)P|\mathcal{G}_{1:K}|)$ flops.

IV. Proposed Detectors

Leveraging the design methodology in [45], we derive next two low-complexity approximations of the GIC-based solution, which avoid the joint search of multiple targets: they are iterative subspace-based algorithms, referred to as the MSD-IS and the MSD-ICM, which extract one target at a time from the measurements. We also illustrate how these solutions can effectively handle small-scale localization errors.

A. Solution Based on the MSD-IS

We propose here to solve a sequence of composite binary hypothesis tests. In each problem, we aim to detect a subspace signal generated by a prospective target in the presence of the subspace interference caused by the previously-detected targets and of the noise.

To proceed, we denote by $\hat{\boldsymbol{x}}^{(k)}$ the estimated position of the target detected in the k-th iteration and by $\mathcal{G}^{(k)}$ the search set in the k-th iteration, with $\mathcal{G}^{(1)} = \mathcal{G}$ and

$$\mathcal{G}^{(k)} = \Big\{\boldsymbol{g} \in \mathcal{G}^{(k-1)} : \min_{i\in\{1,\ldots,k-1\}} \max_{\substack{p\in\{1,\ldots,P\}\\ n\in\{1,\ldots,N\}}} \left|\tau_{p,n}(\boldsymbol{g}) - \tau_{p,n}(\hat{\boldsymbol{x}}^{(i)})\right| > \frac{1}{W}\Big\} \quad (21)$$

for $k \geq 2$. The k-th testing problem is formulated as

$$\begin{cases} \mathcal{H}_0^{(1)} : \boldsymbol{r}_p = \boldsymbol{w}_p,\ \forall\, p \\ \mathcal{H}_1^{(1)} : \boldsymbol{r}_p = \boldsymbol{S}_p(\boldsymbol{x}^{(1)})\boldsymbol{a}_p^{(1)} + \boldsymbol{w}_p,\ \forall\, p \end{cases} \quad (22)$$

if $k = 1$ and

$$\begin{cases} \mathcal{H}_0^{(k)} : \boldsymbol{r}_p = \displaystyle\sum_{i=1}^{k-1} \boldsymbol{S}_p(\hat{\boldsymbol{x}}^{(i)})\boldsymbol{a}_p^{(i)} + \boldsymbol{w}_p,\ \forall\, p \\ \mathcal{H}_1^{(k)} : \boldsymbol{r}_p = \boldsymbol{S}_p(\boldsymbol{x}^{(k)})\boldsymbol{a}_p^{(k)} \\ \qquad\quad + \displaystyle\sum_{i=1}^{k-1} \boldsymbol{S}_p(\hat{\boldsymbol{x}}^{(i)})\boldsymbol{a}_p^{(i)} + \boldsymbol{w}_p,\ \forall\, p \end{cases} \quad (23)$$

if $k \geq 2$, where $\boldsymbol{S}_p(\boldsymbol{x}^{(k)}) \in \mathbb{C}^{M\times N}$ and $\boldsymbol{a}_p^{(k)} = \text{cat}\{a_{p,1}^{(k)}, \ldots, a_{p,N}^{(k)}\} \in \mathbb{C}^N$ are the mode matrix of a prospective target located in $\boldsymbol{x}^{(k)} \in \mathcal{G}^{(k)}$ and the corresponding gain vector, while $\boldsymbol{S}_p(\hat{\boldsymbol{x}}^{(i)}) \in \mathbb{C}^{M\times N}$ and $\boldsymbol{a}_p^{(i)} \in \mathbb{C}^N$ are the mode matrix of the target detected in the i-th iteration and the corresponding gain vector, for $i = 1, \ldots, k-1$. In the following, we treat $\{\boldsymbol{a}_p^{(i)}\}_{i=1}^k$ as unknown deterministic parameters.

The GIC-based rule solving (22) is

$$\max_{\boldsymbol{x}^{(1)}\in\mathcal{G}^{(1)}} \mathcal{J}^{(1)}(\boldsymbol{x}^{(1)}) \underset{\mathcal{H}_0^{(1)}}{\overset{\mathcal{H}_1^{(1)}}{\gtrless}} 0 \quad (24)$$

where

$$\mathcal{J}^{(1)}(\boldsymbol{x}^{(1)}) = \sum_{p=1}^{P} \left(\left\| \boldsymbol{\Pi}_p^{(1)}(\boldsymbol{x}^{(1)})\boldsymbol{C}_p^{-1/2}\boldsymbol{r}_p \right\|^2 - \eta\, \text{rank}\left\{ \boldsymbol{\Pi}_p^{(1)}(\boldsymbol{x}^{(1)}) \right\} \right) \quad (25)$$

and

$$\boldsymbol{\Pi}_p^{(1)}(\boldsymbol{x}^{(1)}) = \boldsymbol{C}_p^{-1/2}\boldsymbol{S}_p(\boldsymbol{x}^{(1)}) \left(\boldsymbol{C}_p^{-1/2}\boldsymbol{S}_p(\boldsymbol{x}^{(1)}) \right)^+. \quad (26)$$

When $\mathcal{H}_1^{(1)}$ is chosen, then the estimated position $\hat{\boldsymbol{x}}^{(1)}$ of the first detected target is the maximizer of (24), while the ML estimate of its gain vector is

$$\hat{\boldsymbol{a}}_p^{(1)} = \left(\boldsymbol{C}_p^{-1/2}\boldsymbol{S}_p(\hat{\boldsymbol{x}}^{(1)}) \right)^+ \boldsymbol{C}_p^{-1/2}\boldsymbol{r}_p. \quad (27)$$

We now tackle the testing problem in (23). For $k \geq 2$, the negative log-likelihood functions under $\mathcal{H}_0^{(k)}$ and $\mathcal{H}_1^{(k)}$ at the p-th receive antenna are

$$-\ln f_{p,0}^{(k)}\left(\boldsymbol{r}_p; \boldsymbol{\alpha}_{p,0}^{(k)}\right) = \ln\left(\pi^M \det \boldsymbol{C}_p\right) + \left\| \boldsymbol{C}_p^{-1/2}\left(\boldsymbol{r}_p - \boldsymbol{\Sigma}_{p,0}^{(k)}\boldsymbol{\alpha}_{p,0}^{(k)}\right) \right\|^2 \quad (28)$$

and

$$-\ln f_{p,1}^{(k)}\left(\boldsymbol{r}_p; \boldsymbol{x}^{(k)}, \boldsymbol{\alpha}_{p,1}^{(k)}\right) = \ln\left(\pi^M \det \boldsymbol{C}_p\right) + \left\| \boldsymbol{C}_p^{-1/2}\left(\boldsymbol{r}_p - \boldsymbol{\Sigma}_{p,1}^{(k)}(\boldsymbol{x}^{(k)})\boldsymbol{\alpha}_{p,1}^{(k)}\right) \right\|^2 \quad (29)$$

respectively, where

$$\boldsymbol{\Sigma}_{p,0}^{(k)} = \left[\boldsymbol{S}_p(\hat{\boldsymbol{x}}^{(1)}) \quad \cdots \quad \boldsymbol{S}_p(\hat{\boldsymbol{x}}^{(k-1)})\right] \in \mathbb{C}^{M\times(k-1)N} \tag{30a}$$

$$\boldsymbol{\alpha}_{p,0}^{(k)} = \text{cat}\left\{\boldsymbol{a}_p^{(1)},\ldots,\boldsymbol{a}_p^{(k-1)}\right\} \in \mathbb{C}^{(k-1)N} \tag{30b}$$

are the augmented mode matrix and gain vector of the interference under $\mathcal{H}_0^{(k)}$, while

$$\boldsymbol{\Sigma}_{p,1}^{(k)}(\boldsymbol{x}^{(k)}) = \left[\boldsymbol{\Sigma}_{p,0}^{(k)} \quad \boldsymbol{S}_p(\boldsymbol{x}^{(k)})\right] \in \mathbb{C}^{M\times kN} \tag{31a}$$

$$\boldsymbol{\alpha}_{p,1}^{(k)} = \text{cat}\left\{\boldsymbol{\alpha}_{p,0}^{(k)},\boldsymbol{a}_p^{(k)}\right\} \in \mathbb{C}^{kN} \tag{31b}$$

are the augmented mode matrix and gain vector accounting for the target and the interference under $\mathcal{H}_1^{(k)}$. Accordingly, the GIC-based rule is

$$\max_{\boldsymbol{x}^{(k)}\in\mathcal{G}^{(k)}} \mathcal{J}^{(k)}(\boldsymbol{x}^{(k)}) \underset{\mathcal{H}_0^{(k)}}{\overset{\mathcal{H}_1^{(k)}}{\gtrless}} 0 \tag{32}$$

where

$$\mathcal{J}^{(k)}(\boldsymbol{x}^{(k)}) = \sum_{p=1}^{P}\Bigg(\ln\frac{f_{p,1}^{(k)}\left(\boldsymbol{r}_p;\boldsymbol{x}^{(k)},\hat{\boldsymbol{\alpha}}_{p,1}^{(k)}(\boldsymbol{x}^{(k)})\right)}{f_{p,0}^{(k)}\left(\boldsymbol{r}_p;\hat{\boldsymbol{\alpha}}_{p,0}^{(k)}\right)} - \eta\left(\text{rank}\left\{\boldsymbol{C}_p^{-1/2}\boldsymbol{\Sigma}_{p,1}^{(k)}(\boldsymbol{x}^{(k)})\right\} - \text{rank}\left\{\boldsymbol{C}_p^{-1/2}\boldsymbol{\Sigma}_{p,0}^{(k)}\right\}\right)\Bigg) \tag{33}$$

and

$$\hat{\boldsymbol{\alpha}}_{p,0}^{(k)} = \left(\boldsymbol{C}_p^{-1/2}\boldsymbol{\Sigma}_{p,0}^{(k)}\right)^{+}\boldsymbol{C}_p^{-1/2}\boldsymbol{r}_p \tag{34a}$$

$$\hat{\boldsymbol{\alpha}}_{p,1}^{(k)}(\boldsymbol{x}^{(k)}) = \left(\boldsymbol{C}_p^{-1/2}\boldsymbol{\Sigma}_{p,1}^{(k)}(\boldsymbol{x}^{(k)})\right)^{+}\boldsymbol{C}_p^{-1/2}\boldsymbol{r}_p \tag{34b}$$

are the ML estimate of the augmented gain vectors at the p-th receive antenna under $\mathcal{H}_1^{(k)}$ and $\mathcal{H}_0^{(k)}$, respectively.

We now elaborate on (33) to obtain some insights into the decision rule in (32). After plugging (34) into the log-likelihood ratio at the p-th receive antenna, we obtain [57]

$$\ln\frac{f_{p,1}^{(k)}\left(\boldsymbol{r}_p;\boldsymbol{x}^{(k)},\hat{\boldsymbol{\alpha}}_{p,1}^{(k)}(\boldsymbol{x}^{(k)})\right)}{f_{p,0}^{(k)}\left(\boldsymbol{r}_p;\hat{\boldsymbol{\alpha}}_{p,0}^{(k)}\right)} = \left\|\boldsymbol{\Pi}_p^{(k)}(\boldsymbol{x}^{(k)})\boldsymbol{C}_p^{-1/2}\boldsymbol{r}_p\right\|^2 \tag{35}$$

where

$$\boldsymbol{\Pi}_p^{(k)}(\boldsymbol{x}^{(k)}) = \left(\boldsymbol{I}_M - \boldsymbol{\Xi}_p^{(k)}\right)\boldsymbol{C}_p^{-1/2}\boldsymbol{S}_p(\boldsymbol{x}^{(k)}) \times\left(\left(\boldsymbol{I}_M - \boldsymbol{\Xi}_p^{(k)}\right)\boldsymbol{C}_p^{-1/2}\boldsymbol{S}_p(\boldsymbol{x}^{(k)})\right)^{+} \tag{36}$$

and

$$\boldsymbol{\Xi}_p^{(k)} = \boldsymbol{C}_p^{-1/2}\boldsymbol{\Sigma}_{p,0}^{(k)}\left(\boldsymbol{C}_p^{-1/2}\boldsymbol{\Sigma}_{p,0}^{(k)}\right)^{+}. \tag{37}$$

Notice here that $\boldsymbol{\Xi}_p^{(k)}$ is the orthogonal projector on the interference subspace spanned by the columns of $\boldsymbol{C}_p^{-1/2}\boldsymbol{\Sigma}_{p,0}^{(k)}$, $\boldsymbol{\Pi}_p^{(k)}(\boldsymbol{x}^{(k)})$ is the orthogonal projector on the part of the column space of $\boldsymbol{C}_p^{-1/2}\boldsymbol{S}_p(\boldsymbol{x}^{(k)})$ not contained in the interference subspace, and $\left\|\boldsymbol{\Pi}_p^{(k)}(\boldsymbol{x}^{(k)})\boldsymbol{C}_p^{-1/2}\boldsymbol{r}_p\right\|^2$ is the energy of the whitened measurement $\boldsymbol{C}_p^{-1/2}\boldsymbol{r}_p$ contained therein. The penalty term at the p-th receive antenna accounts for the dimension of the subspace along with the signal is projected; indeed, we have

$$\begin{aligned}&\text{rank}\left\{\boldsymbol{C}_p^{-1/2}\boldsymbol{\Sigma}_{p,1}^{(k)}(\boldsymbol{x}^{(k)})\right\} - \text{rank}\left\{\boldsymbol{C}_p^{-1/2}\boldsymbol{\Sigma}_{p,0}^{(k)}\right\}\\ &\quad= \text{rank}\left\{\left(\boldsymbol{I}_M - \boldsymbol{\Xi}_p^{(k)}\right)\boldsymbol{C}_p^{-1/2}\boldsymbol{S}_p(\boldsymbol{x}^{(k)})\right\}\\ &\quad= \text{rank}\left\{\boldsymbol{\Pi}_p^{(k)}(\boldsymbol{x}^{(k)})\right\}.\end{aligned} \tag{38}$$

Upon plugging (35) and (38) in (33), we obtain that

$$\mathcal{J}^{(k)}(\boldsymbol{x}^{(k)}) = \sum_{p=1}^{P}\left(\left\|\boldsymbol{\Pi}_p^{(k)}(\boldsymbol{x}^{(k)})\boldsymbol{C}_p^{-1/2}\boldsymbol{r}_p\right\|^2 - \eta\,\text{rank}\left\{\boldsymbol{\Pi}_p^{(k)}(\boldsymbol{x}^{(k)})\right\}\right). \tag{39}$$

The matrix $(\boldsymbol{I}_M - \boldsymbol{\Xi}_p^{(k)})\boldsymbol{C}_p^{-1/2}\boldsymbol{S}_p(\boldsymbol{x}^{(k)})$ may be ill-conditioned if the inspected position $\boldsymbol{x}^{(k)}$ and those of some previously-detected targets present a delay offset less than $1/W$ between the same transmit and the p-th receive antenna; in this case, we can again proceed as in Remark 2 to compute $\boldsymbol{\Pi}_p^{(k)}(\boldsymbol{x}^{(k)})$. Finally, (32) compares the maximum value of the scoring metric in (39) over all points in $\mathcal{G}^{(k)}$ with a threshold. When $\mathcal{H}_1^{(k)}$ is accepted, the estimated position $\hat{\boldsymbol{x}}^{(k)}$ of the k-th detected target is the argument of the maximum, while the ML estimate of the corresponding gain vector is

$$\hat{\boldsymbol{a}}_p^{(k)} = \left(\left(\boldsymbol{I}_M - \boldsymbol{\Xi}_p^{(k)}\right)\boldsymbol{C}_p^{-1/2}\boldsymbol{S}_p(\hat{\boldsymbol{x}}^{(k)})\right)^{+}\boldsymbol{C}_p^{-1/2}\boldsymbol{r}_p. \tag{40}$$

Problems (24) and (32) are sequentially solved for $k = 1, 2, \ldots$ until no additional target is found or there is no remaining grid point to be inspected at the next iteration or $k = K_{\max}$. If the procedure ends at iteration $\hat{K}$, there are $\hat{K}-1$ detected targets if the threshold has not been crossed in the last test, and $\hat{K}$ otherwise. The penalty factor η can be set to maintain a given probability of false alarm, defined here as

$$\text{P}_{\text{fa}} = \text{Pr}\left(\max_{\hat{\boldsymbol{x}}^{(1)}\in\mathcal{G}^{(1)}}\mathcal{J}^{(1)}(\hat{\boldsymbol{x}}^{(1)}) > 0 \text{ under } \mathcal{H}_0^{(1)}\right). \tag{41}$$

The overall procedure is referred to as the MSD-IS and is summarized in Algorithm 1.

B. Solution Based on the MSD-ICM

We discuss here a slight modification of the MSD-IS algorithm, which avoids zero-forcing the subspace signals of the previously-detected targets at each iteration $k \geq 2$; indeed, the zero-forcing operation may cause a detrimental noise enhancement.

To proceed, consider the testing problem in (23) when the gain vectors $\{\boldsymbol{a}_p^{(1)},\ldots,\boldsymbol{a}_p^{(k-1)}\}_{p=1}^{N}$ of the previously-detected targets are modeled as independent circularly-symmetric Gaussian vectors; in particular, assume that $\boldsymbol{a}_p^{(i)}$ has a diagonal covariance

Algorithm 1: Implementation of the MSD-IS/ICM.

provide $\mathcal{G}^{(1)} = \mathcal{G}$, $\hat{K} = 0$ and $\eta \geq 0$
for $k = 1, \ldots, K_{\max}$ **do**
  if $k = 1$ **then**
    Compute $\mathcal{J}^{(1)}(\boldsymbol{x}^{(1)})$ from (25)
  else
    Compute $\mathcal{J}^{(k)}(\boldsymbol{x}^{(k)})$ from (39) or (46) for the MSD-IS or MSD-ICM, respectively
  end if
  if $\max_{\boldsymbol{g} \in \mathcal{G}^{(k)}} \mathcal{J}^{(k)}(\boldsymbol{x}^{(k)}) > 0$ **then**
    Compute $\hat{K} = \hat{K} + 1$
    Compute $\hat{\boldsymbol{x}}^{(k)} = \arg\max_{\boldsymbol{x}^{(k)} \in \mathcal{G}^{(k)}} \mathcal{J}^{(k)}(\boldsymbol{x}^{(k)})$
    Compute $\mathcal{G}^{(k+1)}$ from (21)
    if $\mathcal{G}^{(k+1)} = \emptyset$ **then**
      break
    end if
  else
    break
  end if
end for
return the number of detected targets $\hat{K}$ and, if $\hat{K} \geq 1$, their estimated positions $\{\hat{\boldsymbol{x}}^{(k)}\}_{k=1}^{\hat{K}}$

matrix, denoted by

$$\boldsymbol{\Gamma}_p^{(i)} = \operatorname{diag}\left\{\gamma_{p,1}^{(i)}, \ldots, \gamma_{p,N}^{(i)}\right\} \tag{42}$$

where $\gamma_{p,n}^{(i)} \geq 0$ is a design parameter accounting for the target strength with respect to the receive/transmit antenna pair (p, n). Accordingly, the negative log-likelihood functions under $\mathcal{H}_0^{(k)}$ and $\mathcal{H}_1^{(k)}$ at the p-th receive antenna are

$$-\ln f_{p,0}^{(k)}(\boldsymbol{r}_p) = \ln\left(\pi^M \det \boldsymbol{C}_p^{(k)}\right) + \left\| \left(\boldsymbol{C}_p^{(k)}\right)^{-1/2} \boldsymbol{r}_p \right\|^2 \tag{43}$$

and

$$-\ln f_{p,1}^{(k)}\left(\boldsymbol{r}_p; \boldsymbol{x}^{(k)}, \boldsymbol{a}_p^{(k)}\right) = \ln\left(\pi^M \det \boldsymbol{C}_p^{(k)}\right) + \left\| \left(\boldsymbol{C}_p^{(k)}\right)^{-1/2} \left(\boldsymbol{r}_p - \boldsymbol{S}_p(\boldsymbol{x}^{(k)}) \boldsymbol{a}_p^{(k)}\right) \right\|^2 \tag{44}$$

respectively, where

$$\boldsymbol{C}_p^{(k)} = \sum_{i=1}^{k-1} \boldsymbol{S}_p(\hat{\boldsymbol{x}}^{(i)}) \boldsymbol{\Gamma}_p^{(i)} \boldsymbol{S}_p^H(\hat{\boldsymbol{x}}^{(i)}) + \boldsymbol{C}_p \tag{45}$$

is the interference-plus-noise covariance matrix.

Under the above assumptions, the GIC-based rule is again expressed as in (32), once the scoring metric is computed as

$$\mathcal{J}^{(k)}(\boldsymbol{x}^{(k)}) = \sum_{p=1}^{P} \left(\left\| \tilde{\boldsymbol{\Pi}}_p^{(k)}(\boldsymbol{x}^{(k)}) \left(\boldsymbol{C}_p^{(k)}\right)^{-1/2} \boldsymbol{r}_p \right\|^2 - \eta \operatorname{rank}\left\{ \tilde{\boldsymbol{\Pi}}_p^{(k)}(\boldsymbol{x}^{(k)}) \right\} \right) \tag{46}$$

where

$$\tilde{\boldsymbol{\Pi}}_p^{(k)}(\boldsymbol{x}^{(k)}) = \left(\boldsymbol{C}_p^{(k)}\right)^{-1/2} \boldsymbol{S}_p(\boldsymbol{x}^{(k)}) \times \left(\left(\boldsymbol{C}_p^{(k)}\right)^{-1/2} \boldsymbol{S}_p(\boldsymbol{x}^{(k)}) \right)^{+}. \tag{47}$$

Notice here that $(\boldsymbol{C}_p^{(k)})^{-1/2}\boldsymbol{r}_p$ is the measured data at the p-th receive antenna after an interference-plus-noise whitening transformation, while $\left\|\tilde{\boldsymbol{\Pi}}_p^{(k)}(\boldsymbol{x}^{(k)})(\boldsymbol{C}_p^{(k)})^{-1/2}\boldsymbol{r}_p\right\|^2$ is the energy of $(\boldsymbol{C}_p^{(k)})^{-1/2}\boldsymbol{r}_p$ contained in the column space of $(\boldsymbol{C}_p^{(k)})^{-1/2}\boldsymbol{S}_p(\boldsymbol{x}^{(k)})$. If this latter matrix is ill-conditioned, we can again proceed as in Remark 2 to compute $\tilde{\boldsymbol{\Pi}}_p^{(k)}(\boldsymbol{x}^{(k)})$. When $\mathcal{H}_1^{(k)}$ is accepted, the estimated position $\hat{\boldsymbol{x}}^{(k)}$ of the k-th detected target is obtained from the maximizer of (32), while the ML estimate of its gain vector is

$$\hat{\boldsymbol{a}}_p^{(k)} = \left(\left(\boldsymbol{C}_p^{(k)}\right)^{-1/2} \boldsymbol{S}_p(\hat{\boldsymbol{x}}^{(k)}) \right)^{+} \left(\boldsymbol{C}_p^{(k)}\right)^{-1/2} \boldsymbol{r}_p; \tag{48}$$

also an estimate of the target strength with respect to the receive/transmit antenna pair (p, n) is

$$\gamma_{p,n}^{(k)} = \left|\hat{a}_{p,n}^{(k)}\right|^2. \tag{49}$$

The resulting procedure is referred to as the MSD-ICM and is summarized in Algorithm 1. We underline that the MSD-IS and MSD-ICM algorithms share the same decision logic and also provide the same outcome at the first iteration; they only differ in how the interference from the previously-detected targets is handled in subsequent iterations.

C. Mitigation of Small-Scale Localization Errors

The proposed procedures may be sensitive to off-grid target placements; indeed, the estimated interference subspace at iteration $k \geq 2$ may not fully contain the echoes of the previously-detected targets, thus causing an interference spillover. Next, we give a practical fix involving a modified construction of the interference subspace, which extends the heuristics in [45] to the case where the multiple echoes of each target are produced by different probing signals.

To proceed, denote by $\tilde{\mathcal{G}} \supset \mathcal{G}$ a finer uniform grid with element spacing $\tilde{\Delta}_g \ll \Delta_g$, by $\mathcal{B}^{(i)} = \{\boldsymbol{g} \in \tilde{\mathcal{G}} : \left\|\boldsymbol{g} - \hat{\boldsymbol{x}}^{(i)}\right\| \leq c/W\}$ the set of points in $\tilde{\mathcal{G}}$ *close* to $\hat{\boldsymbol{x}}^{(i)}$, and by $\boldsymbol{E}_{p,n}^{(i)}$ the matrix with columns $\{\boldsymbol{s}_{p,n}(\boldsymbol{g})\}_{\boldsymbol{g} \in \mathcal{B}^{(i)}}$. The MSD-IS algorithm is modified as follows. After noise whitening and interference rejection, at the p-th receive antenna, we assume that the n-th echo of the target detected in the i-th iteration belongs to the augmented subspace spanned by the columns of

$$\left(\boldsymbol{I}_M - \boldsymbol{\Xi}_p^{(i)}\right) \boldsymbol{C}_p^{-1/2} \boldsymbol{E}_{p,n}^{(i)} \tag{50}$$

with the understanding that $\boldsymbol{\Xi}_p^{(i)}$ is an all-zero $M \times M$ matrix for $i = 1$. Since $\boldsymbol{E}_{p,n}^{(i)}$ may contain signatures corresponding to non-resolvable delays, it may be ill-conditioned and some care is required to avoid an unnecessary subspace enlargement. Let $\lambda_{p,n,1}^{(i)}, \ldots, \lambda_{p,n,B^{(i)}}^{(i)}$ be the squared singular values of

$(\boldsymbol{I}_M - \boldsymbol{\Xi}_p^{(i)})\boldsymbol{C}_p^{-1/2}\boldsymbol{E}_{p,n}^{(i)}$ arranged in a decreasing order and let $\boldsymbol{u}_{p,n,1}^{(i)}, \ldots, \boldsymbol{u}_{p,n,B^{(i)}}^{(i)}$ be the corresponding left singular vectors; then, we only retain the left singular vectors corresponding to the $U_{p,n}^{(i)}$ largest singular values, where $U_{p,n}^{(i)} \geq 1$ is the smaller index such that

$$\frac{\left|\hat{a}_{p,n}^{(k)}\right|^2}{|\mathcal{B}^{(i)}|} \sum_{m=U_{p,n}^{(i)}+1}^{|\mathcal{B}^{(i)}|} \lambda_{p,n,m}^{(i)} < \epsilon \tag{51}$$

and ϵ is a design parameter. At this point, the matrix $\boldsymbol{\Xi}_p^{(k)}$ used at the k-th iteration in (36), (39), and (40) is replaced by the orthogonal projector onto the subspace spanned by

$$\left\{ \left\{ \boldsymbol{u}_{p,n,1}^{(i)}, \ldots, \boldsymbol{u}_{p,n,U_{p,n}^{(i)}}^{(i)} \right\}_{n=1}^{N} \right\}_{i=1}^{k-1}. \tag{52}$$

Similarly, at the k-th iteration of the MSD-ICM algorithm, the following augmented covariance matrix

$$\begin{aligned} \boldsymbol{C}_p^{(k)} &= \sum_{i=1}^{k-1} \frac{1}{|\mathcal{B}^{(i)}|} \sum_{\boldsymbol{g} \in \mathcal{B}^{(i)}} \boldsymbol{S}_p(\boldsymbol{g}) \boldsymbol{\Gamma}_p^{(i)} \boldsymbol{S}_p^H(\boldsymbol{g}) + \boldsymbol{C}_p \\ &= \boldsymbol{C}_p^{(k-1)} + \sum_{n=1}^{N} \frac{\gamma_{p,n}^{(k-1)}}{|\mathcal{B}^{(k-1)}|} \boldsymbol{E}_{p,n}^{(k-1)} \left(\boldsymbol{E}_{p,n}^{(k-1)} \right)^H \end{aligned} \tag{53}$$

is used in (46), (47), and (48).

D. Implementation Complexity

Both the MSD-IS and MSD-ICM solutions involve a search over a subset of the grid $\mathcal{G}$ at each iteration, whereby their implementation complexity only scales linearly with the size of $\mathcal{G}$, which is a major cost saving with respect to the GIC-based solution in Section III-B. At the first iteration, both algorithms are equivalent; for a given grid point, the computational burden required to obtain the scoring metric in (25) is dominated by the computation of the orthogonal projector $\boldsymbol{\Pi}_p^{(1)}(\boldsymbol{x}^{(1)})$ for $p = 1, \ldots, P$, which costs at most $\mathcal{O}((M^2N + MN^2)P)$ flops. Consider now the iteration $k \geq 2$. For the MSD-IS algorithm, the computational burden required to obtain the scoring metric in (39) is dominated by the computation of the orthogonal projector $\boldsymbol{\Xi}_p^{(k)}$ for $p = 1, \ldots, P$, which costs at most $\mathcal{O}((M^2(k-1)N + M(k-1)^2\,N^2)P)$ flops; instead, for the MSD-ICM algorithm, the computational burden required to obtain the scoring metric in (46) is dominated by the computation of the square root of the inverse of the matrix $\boldsymbol{C}_p^{(k)}$, for $p = 1, \ldots, P$, which costs at most $\mathcal{O}(M^3P)$flops.

V. Performance Analysis

We consider here a radar employing 2 transmit and 2 receive antennas, with the system parameters in Table I and the geometry in Fig. 3. The targets are located in the inspected region $\mathbb{Y} = [5700, 6200] \times [5700, 6200]$ m^2. The time-coded waveforms in (1) are used, with randomly-generated four-phase code sequences, $\psi(t) = \Pi(t/T_c)$, and $\phi(t) = \sqrt{1/T_c}\Pi(t/T_c)$. We denote the k-th target by Q_k and model its response along

TABLE I
System Parameters

F_s 20 MHz	W 10 MHz	$\mathrm{P_{fa}}$ 2.5×10^{-3}	L 64
T_s 0.05 us	T_c, T_ψ 0.1 us	T 6.4 us	T_{pri} 24 us
Range bin 15 m	Δ_g 10 m	$\tilde{\Delta}_g$ 0.05 m	$K_{\max}$ 20

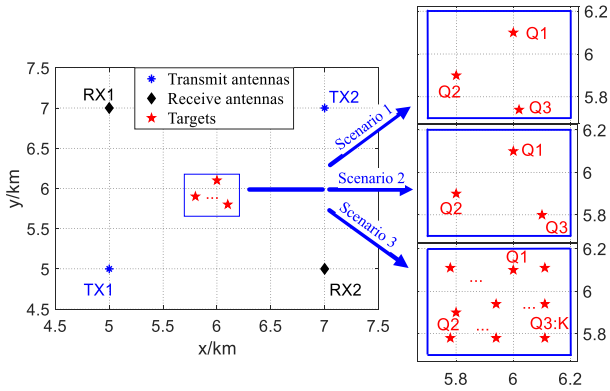

Fig. 3. The 3 km × 3 km plane involving four antennas and multiple targets for three different scenarios. The transmit antennas are placed at $\boldsymbol{x}_1^{\mathrm{tx}} = (5000, 5000)$ m, $\boldsymbol{x}_2^{\mathrm{tx}} = (7000, 7000)$ m, while the receive antennas at $\boldsymbol{x}_1^{\mathrm{rx}} = (5000, 7000)$ m, $\boldsymbol{x}_2^{\mathrm{rx}} = (7000, 5000)$ m.

the path $\mathrm{TX}_n - \mathrm{Q}_k - \mathrm{RX}_p$ as

$$a_{p,n,k} = \mathrm{e}^{-j\phi_{p,n,k}} \sqrt{\zeta_{p,n,k}} \tag{54}$$

where $\phi_{p,n,k}$ is a uniform random phase and $\zeta_{p,n,k}$ accounts for the antenna gain, the target radar cross-section, and the propagation effects; also, we define its SNR as

$$\mathrm{SNR}_k = \frac{1}{NP} \sum_{n=1}^{N} \sum_{p=1}^{P} |a_{p,n,k}|^2 \|\boldsymbol{C}_{w,p}^{-1/2} \boldsymbol{s}_{p,n}(\boldsymbol{x}_k)\|^2. \tag{55}$$

Finally, we denote the ratio between the SNR of the targets Q_k and Q_q as $\mu_{k,q}^2 = \mathrm{SNR}_k/\mathrm{SNR}_q$.

Three configurations are studied in the following, as shown in Fig. 3. Targets Q_1 and Q_2 are always kept at $\boldsymbol{x}_1 = (6000, 6100)$ m and $\boldsymbol{x}_2 = (5800, 5900)$ m, respectively, so that their echoes are resolvable for each receive/transmit antenna pair, and have $\mu_{2,1} = 0.5$. Instead, targets $\mathrm{Q}_3, \ldots, \mathrm{Q}_K$ have a different position and strength in the considered scenarios (more on this infra). Target Q_1 is the target of interest, and its probability of detection ($\mathrm{P_d}$) and the root mean square error (RMSE) in the estimation of its position are used as relevant performance metrics. In particular, under $\bar{\mathcal{H}}_0$, we say target Q_1 is detected if the event $E_1 = \{\exists\, k \in \{1, \ldots, \hat{K}\} : \|\hat{\boldsymbol{x}}^{(k)} - \boldsymbol{x}_1\| \leq c/W\}$ is true; accordingly, we have

$$P_d = \mathbb{P}\left(E_1 \mid \bar{\mathcal{H}}_0\right) \tag{56a}$$

$$\mathrm{RMSE} = \sqrt{\mathbb{E}\left[\min_{k \in \{1, \ldots \hat{K}\}} \|\hat{\boldsymbol{x}}^{(k)} - \boldsymbol{x}_1\|^2 \mid E_1, \bar{\mathcal{H}}_0 \right]}. \tag{56b}$$

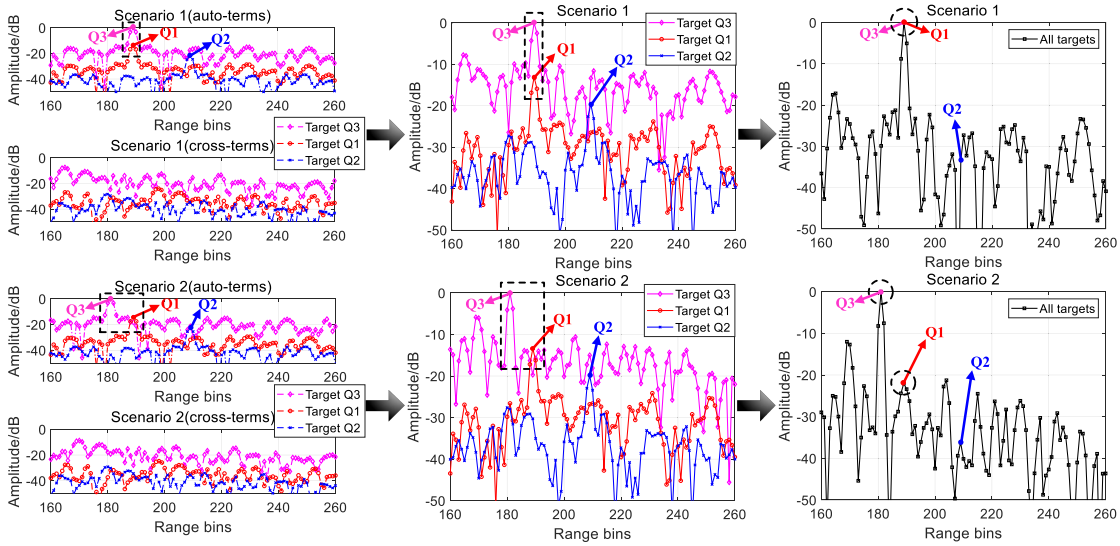

Fig. 4. Normalized noise-free output of a correlator matched to the waveform emitted by TX_2 when the signal received by RX_2 is at the input. The left plot shows the output auto-correlation for each target echo produced by $s_2(t)$ (auto-terms) and the output cross-correlation for each target echo produced by $s_1(t)$ (cross-terms); the middle plots report the superposition of the auto- and cross-terms for each target; the right plots report the overall output obtained by superimposing all contributions. The top and bottom plots refer to Scenarios 1 and 2 in Fig. 3, respectively, when $\mu_{2,1} = 0.5$ and $\mu_{3,1} = 4.75$.

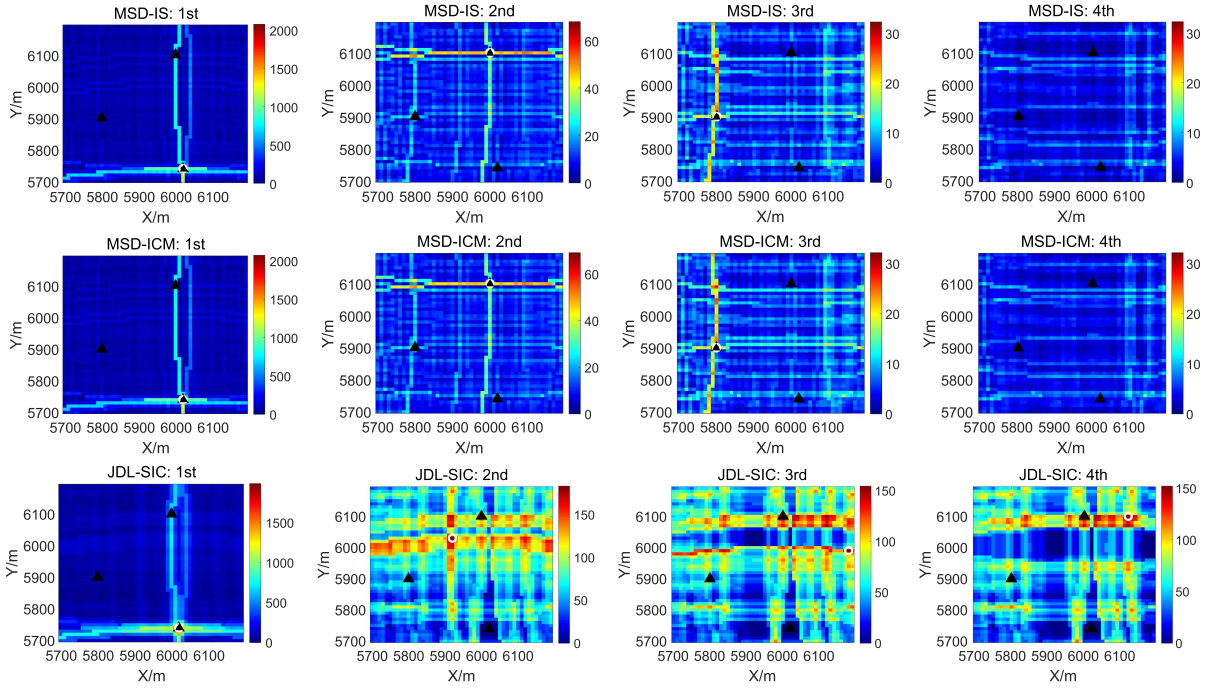

Fig. 5. Output data plane of the MSD-IS (top), MSD-ICM (middle), and JDL-SIC solutions (bottom) in four consecutive iterations (from left to right). The triangle markers are the true target positions; the circle marker is the estimated position of the target detected (if any) in each iteration. Scenario 1 in Fig. 3 is considered with $\text{SNR}_1 = 14$ dB, $\mu_{2,1} = 0.5$, and $\mu_{3,1} = 4.75$.

Three benchmarks are considered for comparison. The first one is the JDL procedure with successive interference cancellation (JDL-SIC) in [30]; the second one is the GLRT detector operating in the absence of the interfering targets (namely, $Q_2, \ldots, Q_K$), referred to as GLRT with cleaned data (GLRT-CD); the third one is the GLRT with known locations of the interfering targets (GLRT-KL). All results are obtained by averaging over 2×10^4 independent instances and have been obtained by using the software MATLAB 2021a and a machine with two 2.5 GHz Intel(R) Xeon(R) E5-2678V3 CPUs.

A. *Scenario 1: Impact of Target Strength*

Consider here the Scenario 1 in Fig. 3, where target Q_3 is located at $\boldsymbol{x}_3 = (6020, 5740)$ m. Under this setting, the targets are *partially-separable*, as their echoes are resolvable for each

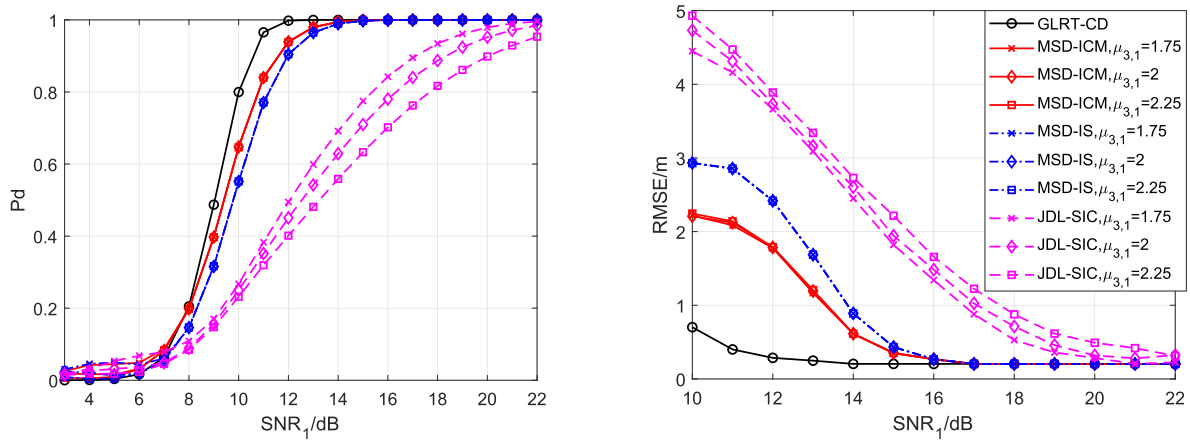

Fig. 6. P_d (left) and RMSE in the position estimate (right) of target Q_1 versus SNR_1. Scenario 1 in Fig. 3 is considered with $\mu_{2,1} = 0.5$ and different values of $\mu_{3,1}$.

receive/transmit antenna pair, except for those two along the paths $TX_2 - Q_1 - RX_2$ and $TX_2 - Q_3 - RX_2$. To illustrate the sidelobe masking resulting from the imperfect auto- and cross-correlation functions of the adopted waveforms, we analyze in Fig. 4 (top), the normalized noise-free output of a standard correlator matched to $s_2(t)$, when the signal $r_2(t)$ observed by RX_2 is at the input and $\mu_{3,1} = 4.75$. In particular, the left plot shows the output auto-correlation for each target echo produced by $s_2(t)$ (auto-terms) and the output cross-correlation for each target echo produced by $s_1(t)$ (cross-terms); also, the middle plot reports the superposition of the auto- and cross-terms for each target; finally, the right plot reports the overall output obtained by superimposing all contributions. It is seen by inspection that the echos of targets Q_1 and Q_3 are not resolvable through the receive/transmit antenna pair (2, 2) and that target Q_2 is masked by the range sidelobes of the target Q_3.

Next, we illustrate the evolution of the proposed solutions in a single snapshot. The output data plane (i.e., the value of the scoring metric over $\mathbb{Y}$) is reported in Fig. 5 for the MSD-IS, MSD-ICM, and JDL-SIC solutions over four iterations, when $SNR_1 = 14$ dB and $\mu_{3,1} = 4.75$. The following remarks are now in order.

- At the 1-st iteration, all scoring metrics peak at the true position of target Q_3, so that all algorithms can detect and localize the strongest target; however, target Q_3 is also responsible for the presence here of large sidelobes.
- At the 2-nd iteration, an erroneous decision is made by the JDL-SIC algorithm, as there are many areas in $\mathbb{Y}$ where the value of its scoring metric is larger than that at the true positions of targets Q_1 and Q_2; the reason is that this algorithm neglects at the design stage the sidelobe interference from the first detected target; however, such interference is here strong enough to mask the other two targets. A similar issue is present at the 3-rd iteration of the JDL-SIC algorithm.
- The MSD-IS and MSD-ICM algorithms can instead detect and localize all targets; the reason is that they are explicitly designed to mitigate the interference from the previously detected targets at each iteration, thus overcoming the aforementioned masking effects.

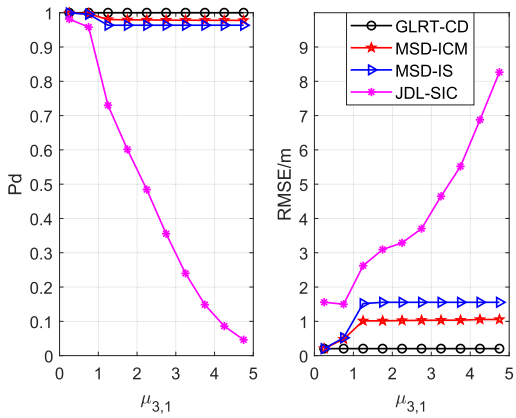

Fig. 7. P_d (left) and RMSE in the position estimate (right) of target Q_1 versus $\mu_{3,1}$. Scenario 1 in Fig. 3 is considered with $SNR_1 = 13$ dB and $\mu_{2,1} = 0.5$.

Finally, Figs. 6 and 7 report P_d and RMSE in the position estimate of target Q_1 versus SNR_1 and $\mu_{3,1}$, respectively. The proposed algorithms perform only slightly worse than the single-target benchmark and are not significantly affected by the strength of target Q_3: this confirms their capability of detecting and localizing multiple targets even in the presence of a power imbalance and partially overlapped subspaces. The MSD-ICM slightly outperforms the MSD-IS here, as the latter suffers from a larger noise enhancement when canceling the interference caused by the previously-detected targets. On the other hand, the performance of the JDL-SIC rapidly degrades as $\mu_{3,1}$ increases, as this solution neglects the cross- and auto-terms at the output of the MF.

B. Scenario 2: Impact of Target Separation

We now consider the Scenario 2 in Fig. 3, where target Q_3 is located at $\boldsymbol{x}_3 = (6100, 5800)$ m. Under this setting, the target echoes are resolvable for each receive/transmit antenna pair

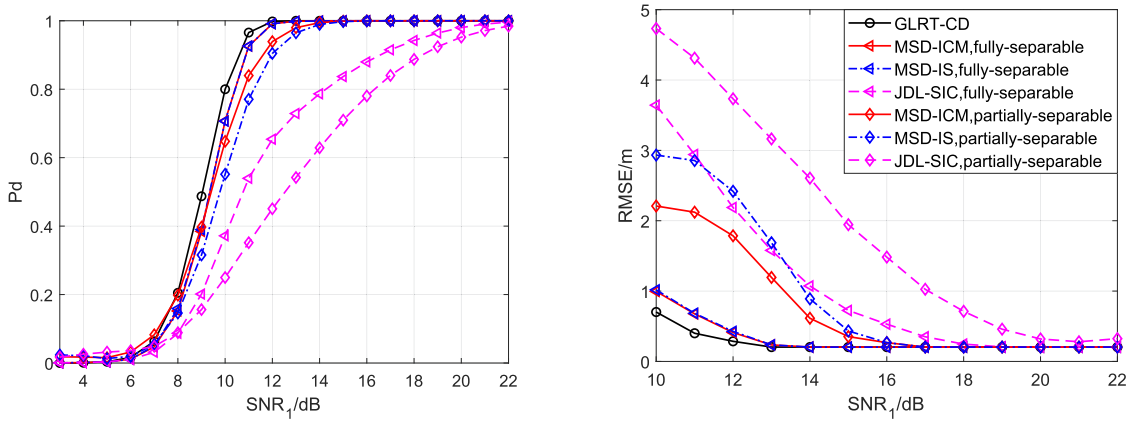

Fig. 8. P_d (left) and RMSE in the position estimate (right) of target Q_1 versus SNR_1. Scenario 1 (*partially-separable* targets) and 2 (*fully-separable* targets) in Fig. 3 are considered with $\mu_{2,1} = 0.5$ and $\mu_{3,1} = 2$.

(i.e., we have *fully-separable* targets). In order to verify this latter point, Fig. 4 (bottom) reports the normalized noise-free output of a standard correlator matched to the waveform $s_2(t)$ emitted by TX_2, when the signal $r_2(t)$ observed by RX_2 is at the input, $\mu_{2,1} = 0.5$, and $\mu_{3,1} = 4.75$. Unlike the Scenario 1, targets Q_1 and Q_3 are now seen in different range bins through the receive/transmit antenna pair $(2, 2)$; however, the two weaker targets are again masked by the strongest one.

Fig. 8 compares the detection and localization performance for *partially-separable* (Scenario 1) and *fully-separable* (Scenario 2) targets when $\mu_{2,1} = 0.5$ and $\mu_{3,1} = 2$. All algorithms perform better in the presence of *fully-separable* targets: indeed, when Q_3 is detected before Q_1, the subsequent interference mitigation step no longer cancels the echoes of Q_1 along the path $TX_2 - RX_2$. Remarkably, for the *fully-separable* case, the proposed solutions only present here an SNR loss of 0.45 dB with respect to the single-target GLRT-CD benchmark when $P_d = 0.8$; instead, the performance of the JDL-SIC still remains much worse.

C. Scenario 3: Impact of Target Number

Finally, we consider the Scenario 3 in Fig. 3, where targets $Q_3, \ldots, Q_K$ are randomly displaced in $\mathbb{Y}$ with $SNR_1 = 13$ dB, $\mu_{2,1} = 0.5$, and $SNR_k \in [25, 50]$ dB for $k = 3, \ldots, K$. Fig. 9 reports P_d and RMSE in the position estimate of target Q_1 versus K. It can be seen that the performance of the proposed algorithms gracefully degrades with an increasing number of interfering targets (as opposed to the JDL-SIC), thus confirming their robustness to the sidelobe masking problem. The performance of the genie-aided solution GLRT-KL also degrades when K is increased; indeed, even when the interference from the other targets belongs to a known subspace, its elimination still may take away a part of the signal of interest. Interestingly, in the considered scenario, the proposed solutions present a relevant performance loss, as compared to the GLRT-KL benchmark, only when the number of overall targets K is above 10.

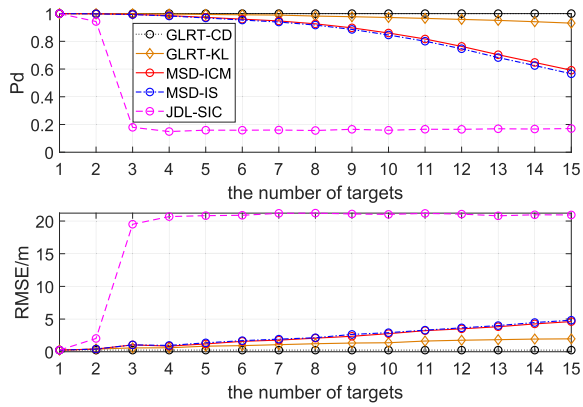

Fig. 9. P_d (top) and RMSE (bottom) in the position estimate of target Q_1 versus K. Scenario 3 in Fig. 3 is considered with $SNR_1 = 13$ dB, $\mu_{2,1} = 0.5$, and $SNR_k \in [25, 50]$ dB for $k = 3, \ldots, K$.

VI. Conclusion

In this article, we have addressed the problem of multi-target JDL in a distributed MIMO radar employing waveforms with imperfect auto- and cross-correlation functions, which can be recast as a composite multiple hypothesis testing problem. After modeling the signals at each receive antenna as the superposition of an unknown number of subspace signals and noise, we have shown that the JDL of multiple targets is tantamount to a joint model order selection and subspace matching problem, which can be tackled by resorting to a GIC. To limit the computational cost, we have then derived two approximate solutions, which convert the joint multi-target search into a sequence of single-target searches. A numerical study has been provided to demonstrate the effectiveness of our solutions under diverse instances of the target strength, separation, and number, also in comparison with another recently deployed algorithm, the single-target benchmark, and an ideal solution that has perfect knowledge of the numbers of interfering targets and their locations.

Future works may consider distributed radar networks with partial/no knowledge of the noise covariance matrices; the development of distributed algorithms for reducing the information exchange among the receive antennas may also be considered. Finally, the derivation of the Cramér-Rao bounds for the considered multi-target joint detection and localization problem still remains an open problem.

REFERENCES

[1] E. Fishler, A. Haimovich, R. Blum, D. Chizhik, L. Cimini, and R. Valenzuela, "MIMO radar: An idea whose time has come," in *Proc. IEEE Radar Conf.*, 2004, pp. 71–78.

[2] J. Li and P. Stoica, "MIMO radar with colocated antennas," *IEEE Signal Process. Mag.*, vol. 24, no. 5, pp. 106–114, Sep. 2007.

[3] A. M. Haimovich, R. S. Blum, and L. J. Cimini, "MIMO radar with widely separated antennas," *IEEE Signal Process. Mag.*, vol. 25, no. 1, pp. 116–129, 2008.

[4] N. H. Lehmann et al., "Evaluation of transmit diversity in MIMO-radar direction finding," *IEEE Trans. Signal Process.*, vol. 55, no. 5, pp. 2215–2225, May 2007.

[5] Z. Cheng, Z. He, S. Zhang, and J. Li, "Constant moduluswaveform design for MIMO radar transmit beampattern," *IEEE Trans. Signal Process.*, vol. 65, no. 18, pp. 4912–4923, Sep. 2017.

[6] P. Chen, L. Zheng, X. Wang, H. Li, and L. Wu, "Moving target detection using colocated MIMO radar on multiple distributed moving platforms," *IEEE Trans. Signal Process.*, vol. 65, no. 17, pp. 4670–4683, Sep. 2017.

[7] S. Yang, W. Yi, A. Jakobsson, Y. Wang, and H. Xiao, "Weak signal detection with low-bit quantization in colocated MIMO radar," *IEEE Trans. Signal Process.*, vol. 71, pp. 447–460, 2023.

[8] L. Lan, M. Rosamilia, A. Aubry, A. De Maio, G. Liao, and J. Xu, "Adaptive target detection with polarimetric FDA-MIMO radar," *IEEE Trans. Aerosp. Electron. Syst.*, vol. 59, no. 3, pp. 2204–2220, Jun. 2023.

[9] E. Fishler, A. Haimovich, R. S. Blum, L. J. Cimini, D. Chizhik, and R. A. Valenzuela, "Spatial diversity in radars–models and detection performance," *IEEE Trans. Signal Process.*, vol. 54, no. 3, pp. 823–838, Mar. 2006.

[10] Q. He and R. S. Blum, "Diversity gain for MIMO neyman–pearson signal detection," *IEEE Trans. Signal Process.*, vol. 59, no. 3, pp. 869–881, Mar. 2011.

[11] M. Sadeghi, F. Behnia, R. Amiri, and A. Farina, "Target localization geometry gain in distributed MIMO radar," *IEEE Trans. Signal Process.*, vol. 69, pp. 1642–1652, 2021.

[12] Q. He, N. H. Lehmann, R. S. Blum, and A. M. Haimovich, "MIMO radar moving target detection in homogeneous clutter," *IEEE Trans. Aerosp. Electron. Syst.*, vol. 46, no. 3, pp. 1290–1301, Jul. 2010.

[13] P. Wang, H. Li, and B. Himed, "Moving target detection using distributed MIMO radar in clutter with nonhomogeneous power," *IEEE Trans. Signal Process.*, vol. 59, no. 10, pp. 4809–4820, Oct. 2011.

[14] S. Zhou and H. Liu, "Space-partition-based target detection for distributed MIMO radar," *IEEE Trans. Aerosp. Electron. Syst.*, vol. 49, no. 4, pp. 2717–2729, Oct. 2013.

[15] M. Dianat, M. R. Taban, J. Dianat, and V. Sedighi, "Target localization using least squares estimation for MIMO radars with widely separated antennas," *IEEE Trans. Aerosp. Electron. Syst.*, vol. 49, no. 4, pp. 2730–2741, Oct. 2013.

[16] C.-H. Park and J.-H. Chang, "Closed-form localization for distributed MIMO radar systems using time delay measurements," *IEEE Trans. Wireless Commun.*, vol. 15, no. 2, pp. 1480–1490, Feb. 2016.

[17] R. Amiri, F. Behnia, and M. A. M. Sadr, "Exact solution for elliptic localization in distributed MIMO radar systems," *IEEE Trans. Veh. Technol.*, vol. 67, no. 2, pp. 1075–1086, Feb. 2018.

[18] M. Xie, W. Yi, L. Kong, and T. Kirubarajan, "Receive-beam resource allocation for multiple target tracking with distributed MIMO radars," *IEEE Trans. Aerosp. Electron. Syst.*, vol. 54, no. 5, pp. 2421–2436, Oct. 2018.

[19] Y. Wang, T. Zhou, and W. Yi, "Geometric optimization of distributed MIMO radar system for accurate localization in multiple key subareas," *Signal Process.*, vol. 201, 2022, Art. no. 108689.

[20] Q. He, R. S. Blum, H. Godrich, and A. M. Haimovich, "Target velocity estimation and antenna placement for MIMO radar with widely separated antennas," *IEEE J. Sel. Topics Signal Process.*, vol. 4, no. 1, pp. 79–100, Feb. 2010.

[21] H. Zhang, W. Liu, Z. Zhang, W. Lu, and J. Xie, "Joint target assignment and power allocation in multiple distributed MIMO radar networks," *IEEE Syst. J.*, vol. 15, no. 1, pp. 694–704, Mar. 2021.

[22] M. M. Naghsh, M. Modarres-Hashemi, M. A. Kerahroodi, and E. H. M. Alian, "An information theoretic approach to robust constrained code design for MIMO radars," *IEEE Trans. Signal Process.*, vol. 65, no. 14, pp. 3647–3661, Jul. 2017.

[23] H. Godrich, A. Haimovich, and R. S. Blum, "Target localisation techniques and tools for multiple-input multiple-output radar," *IET Radar, Sonar Navigation*, vol. 3, no. 4, pp. 314–327, Aug. 2009.

[24] H. Godrich, A. M. Haimovich, and R. S. Blum, "Target localization accuracy gain in MIMO radar-based systems," *IEEE Trans. Inf. Theory*, vol. 56, no. 6, pp. 2783–2803, Jun. 2010.

[25] Q. He, R. S. Blum, and A. M. Haimovich, "Noncoherent MIMO radar for location and velocity estimation: More antennas means better performance," *IEEE Trans. Signal Process.*, vol. 58, no. 7, pp. 3661–3680, Jul. 2010.

[26] O. Bar-Shalom and A. J. Weiss, "Direct positioning of stationary targets using MIMO radar," *Signal Process.*, vol. 91, no. 10, pp. 2345–2358, Oct. 2011.

[27] R. Niu, R. S. Blum, P. K. Varshney, and A. L. Drozd, "Target localization and tracking in noncoherent multiple-input multiple-output radar systems," *IEEE Trans. Aerosp. Electron. Syst.*, vol. 48, no. 2, pp. 1466–1489, Apr. 2012.

[28] G. Zhang, W. Yi, P. K. Varshney, and L. Kong, "Direct target localization with quantized measurements in non-coherent distributed MIMO radar systems," *IEEE Trans. Geosci. Remote Sens.*, vol. 61, 2023, Art. no. 5103618.

[29] S. Yang, W. Yi, and A. Jakobsson, "Multitarget detection strategy for distributed MIMO radar with widely separated antennas," *IEEE Trans. Geosci. Remote Sens.*, vol. 60, 2022, Art. no. 5113516.

[30] W. Yi, T. Zhou, Y. Ai, and R. S. Blum, "Suboptimal low complexity joint multi-target detection and localization for non-coherent MIMO radar with widely separated antennas," *IEEE Trans. Signal Process.*, vol. 68, pp. 901–916, 2020.

[31] L. Zhu, G. Wen, Y. Liang, D. Luo, and H. Jian, "Multitarget enumeration and localization in distributed MIMO radar based on energy modeling and compressive sensing," *IEEE Trans. Aerosp. Electron. Syst.*, vol. 59, no. 4, pp. 4493–4510, Aug. 2023.

[32] C. Ma, T. S. Yeo, C. S. Tan, Y. Qiang, and T. Zhang, "Receiver design for MIMO radar range sidelobes suppression," *IEEE Trans. Signal Process.*, vol. 58, no. 10, pp. 5469–5474, Oct. 2010.

[33] Y. I. Abramovich and G. J. Frazer, "Bounds on the volume and height distributions for the MIMO radar ambiguity function," *IEEE Signal Process. Lett.*, vol. 15, pp. 505–508, 2008.

[34] Y. Zhao, X. Lu, M. Ritchie, W. Su, and H. Gu, "Suppression of sidelobes in MIMO radar with distinctive piecewise non-linear frequency modulation sub-carrier," *Int. J. Remote Sens.*, vol. 41, no. 1, pp. 353–372, Jul. 2019.

[35] P. Wang and H. Li, "Target detection with imperfect waveform separation in distributed MIMO radar," *IEEE Trans. Signal Process.*, vol. 68, pp. 793–807, Jan. 2020.

[36] H. Li, F. Wang, C. Zeng, and M. Govoni, "Signal detection in distributed MIMO radar with non-orthogonal waveforms and sync errors," *IEEE Trans. Signal Process.*, vol. 69, pp. 3671–3684, 2021.

[37] C. Zeng, F. Wang, H. Li, and M. A. Govoni, "Delay compensation for distributed MIMO radar with non-orthogonal waveforms," *IEEE Signal Process. Lett.*, vol. 29, pp. 41–45, 2022.

[38] X. Lu, B. Xu, T.-S. Yeo, W. Su, and H. Gu, "Co-located MIMO radar target detection in cluttered and noisy environment based on 2D block sparse recovery," *IEEE Trans. Signal Process.*, vol. 69, pp. 3431–3445, 2021.

[39] M. F. Keskin, H. Wymeersch, and V. Koivunen, "MIMO-OFDM joint radar-communications: Is ICI friend or foe?," *IEEE J. Sel. Topics Signal Process.*, vol. 15, no. 6, pp. 1393–1408, Nov. 2021.

[40] F. Colone, C. Palmarini, T. Martelli, and E. Tilli, "Sliding extensive cancellation algorithm for disturbance removal in passive radar," *IEEE Trans. Aerosp. Electron. Syst.*, vol. 52, no. 3, pp. 1309–1326, Jun. 2016.

[41] G. Paolo Blasone, F. Colone, P. Lombardo, P. Wojaczek, and D. Cristallini, "Passive radar DPCA schemes with adaptive channel calibration," *IEEE Trans. Aerosp. Electron. Syst.*, vol. 56, no. 5, pp. 4014–4034, Oct. 2020.

[42] E. Grossi, M. Lops, and L. Venturino, "An iterative interference cancellation algorithm for opportunistic sensing in IEEE 802.11ad networks," in *Proc. IEEE 8th Int. Workshop Comput. Adv. Multi-Sensor Adaptive Process.*, 2019, pp. 141–145.

[43] E. Grossi, M. Lops, and L. Venturino, "Adaptive detection and localization exploiting the IEEE 802.11ad standard," *IEEE Trans. Wireless Commun.*, vol. 19, no. 7, pp. 4394–4407, Jul. 2020.

[44] E. Grossi, M. Lops, A. M. Tulino, and L. Venturino, "Extended target detection and localization in 802.11ad/y radars," in *Proc. IEEE Radar Conf.*, 2020, pp. 1–5.

[45] E. Grossi, M. Lops, A. M. Tulino, and L. Venturino, "Opportunistic sensing using mmWave communication signals: A subspace approach," *IEEE Trans. Wireless Commun.*, vol. 20, no. 7, pp. 4420–4434, Jul. 2021.

[46] P. Stoica and Y. Selen, "Model-order selection: A review of information criterion rules," *IEEE Signal Process. Mag.*, vol. 21, no. 4, pp. 36–47, Jul. 2004.
[47] Y. Lai, L. Venturino, E. Grossi, and W. Yi, "Subspace-based detection and localization in distributed MIMO radars," in *Proc. IEEE 12th Sensor Array Multichannel Signal Process. Workshop*, 2022, pp. 365–369.
[48] D. Slepian, "On bandwidth," *Proc. IEEE*, vol. 64, no. 3, pp. 292–300, Mar. 1976.
[49] N. Levanon and E. Mozeson, *Radar Signals*. Hoboken, NJ, USA: Wiley, 2004.
[50] C. Sturm and W. Wiesbeck, "Waveform design and signal processing aspects for fusion of wireless communications and radar sensing," *Proc. IEEE*, vol. 99, no. 7, pp. 1236–1259, Jul. 2011.
[51] J. Proakis and M. Salehi, *Digital Communications*, 5th ed. New York, NY, USA: McGraw Hill, 2014.
[52] S. D. Blunt and E. L. Mokole, "Overview of radar waveform diversity," *IEEE Aerosp. Electron. Syst. Mag.*, vol. 31, no. 11, pp. 2–42, Nov. 2016.
[53] M. Bică and V. Koivunen, "Generalized multicarrier radar: Models and performance," *IEEE Trans. Signal Process.*, vol. 64, no. 17, pp. 4389–4402, Sep. 2016.
[54] X. Ouyang and J. Zhao, "Orthogonal chirp division multiplexing," *IEEE Trans. Commun.*, vol. 64, no. 9, pp. 3946–3957, Sep. 2016.
[55] R. G. Gallager, *Stochastic processes, theory for applications*. Cambridge, U.K.: Cambridge Univ. Pres, 2013.
[56] P. Stoica, Y. Selen, and J. Li, "On information criteria and the generalized likelihood ratio test of model order selection," *IEEE Signal Process. Lett.*, vol. 11, no. 10, pp. 794–797, Oct. 2004.
[57] L. L. Scharf and B. Friedlander, "Matched subspace detectors," *IEEE Trans. Signal Process.*, vol. 42, no. 8, pp. 2146–2157, Aug. 1994.

Yangming Lai (Student Member, IEEE) received the B.E. degree from the University of Electronic Science and Technology of China, Chengdu, China, in 2018, where he is currently working toward the Ph.D. degree in information and communication engineering. Since October 2022, he has been a Visiting Ph.D. Student with the Communication Systems Group, Department of Electrical Engineering, Chalmers University of Technology, Gothenburg, Sweden, under the financial support from the China Scholarship Council. His research interests include statistical signal processing, radar signal processing, and joint radar-communications, especially target detection and localization technology.

Luca Venturino (Senior Member, IEEE) received the "Laurea" degree in telecommunications engineering and the Ph.D. degree in electrical engineering from the University of Cassino and Southern Lazio, Cassino, Italy. He is currently an Associate Professor with the Department of Electrical and Information Engineering, the University of Cassino and Southern Lazio. In 2004, 2009, and 2022, he was Visiting Scholar with the Columbia University, New York, NY, USA. Between 2006 and 2008, he spent nine months with NEC Laboratories America, Princeton, NJ, USA, as Research Associate. His research interests include the general areas of signal processing and resource allocation for wireless communications and radars. He was an Associate Editor for the IEEE SIGNAL PROCESSING LETTERS and IEEE TRANSACTIONS ON SIGNAL PROCESSING and the Senior Area Editor of the IEEE SIGNAL PROCESSING LETTERS. He is currently the Senior Area Editor of the IEEE TRANSACTIONS ON SIGNAL PROCESSING.

Emanuele Grossi (Senior Member, IEEE) received the Dr. Eng. degree in telecommunication engineering in 2002 and the Ph.D. degree in electrical engineering in 2006 from the University of Cassino and Southern Lazio, Cassino, Italy. He is currently an Associate Professor with the Department of Electrical and Information Engineering, University of Cassino and Southern Lazio. In 2005, he was visiting Scholar with the Department of Electrical and Computer Engineering, The University of British Columbia, Vancouver, BC, Canada, and in 2009 he had a visiting appointment in the Digital Technology Center, University of Minnesota, Minneapolis, MN, USA. His research interests include detection and estimation, with emphasis on communications and radar signal processing. He is an Associate Editor for the IEEE TRANSACTIONS ON SIGNAL PROCESSING and *EURASIP Signal Processing*, Elsevier.

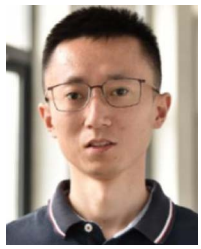

Wei Yi (Senior Member, IEEE) received the B.E. and Ph.D. degrees in electronic engineering from the University of Electronic Science and Technology of China, Chengdu, China, in 2006 and 2012, respectively. From 2010 to 2012, he was a Visiting Student with the Melbourne Systems Laboratory, University of Melbourne, Melbourne, VIC, Australia. Since 2012, he has been with the University of Electronic Science and Technology of China, where he is currently a Full Professor with the School of Information and Communication Engineering. His research interests include target detection and tracking, radar signal processing, multi-sensor information fusion, and resources management. Dr. Yi was the recipient of the Best Student article Competition-First place winner at the 2012 IEEE Radar Conference, Atlanta, Best Student article Award at the 15th FUSION Conference, Singapore, 2012, and also the co-recipient of the Best Student article Award at the 21st FUSION Conference, Cambridge, 2018. He is a Member of the Editorial Boards of the *Journal of Radars*. He was the Guest Editor of the MDPI *Sensors* and *Frontiers of Information Technology and Electronic Engineering*. He was also the General Co-Chair of ICCAIS 2019 and TPC Member of international conferences, such as IEEE Radar Conference and FUSION Conference.

Open Access provided by 'Università degli Studi di Cassino e del Lazio Meridionale' within the CRUI CARE Agreement